University of Nevada, Reno

Damped Vibration Sensing Using Optical Fiber Resonator Method

A Thesis submitted in partial fulfillment of the requirements for the degree of Masters of Science in Electrical Engineering

By

Prachi Bhide

Dr.Banmali Rawat/Thesis Advisor

May 2012

University of Nevada, Reno
Statewide • Worldwide

THE GRADUATE SCHOOL

We recommend that the thesis
prepared under our supervision by

PRACHI BHIDE

entitled

Damped Vibration Sensing Using Optical Fiber Resonator Method

be accepted in partial fulfillment of the
requirements for the degree of

MASTER OF SCIENCE

Dr. Banmali Rawat, Advisor

Dr. Xiaoshan Zhu , Committee Member

Dr. Aaron Covington, Graduate School Representative

Marsha H. Read, Ph. D., Dean, Graduate School

May, 2012

Abstract

In past few years the demand for fiber optic vibration sensors has increased as they are free from electromagnetic interference (EMI) and chemical corrosion. These sensors have been widely used for monitoring earthquakes, hydroelectric dam, and structural damages in bridges and highways. This research presents a new method which implements a multilongitudinal mode fiber laser (MLMFL) to detect damped vibrations. MLMFL is made up of Single mode fiber (SMF), Erbium doped fiber (EDF), Fiber Bragg grating (FBG) and 3dB coupler forms a resonant cavity. The EDF provides gain for the cavity. When light with a wavelength of 980nm pump power is launched into the resonant cavity, multilongitudinal modes are produced within the reflected bandwidth of the FBG. Several beat frequency signals are produced by beating any two modes in the resonant cavity. When damped vibrations are applied, the strain experienced by the fiber changes the length of the cavity which changes the beat frequency. Thus by measuring the change in beat frequency of the resonant cavity the damped vibration frequencies are measured through proper calibration. Damped vibration frequencies were modeled using analytical simulations to compare with those measured experimentally. From analytical simulations, the damped vibration frequencies are observed from 500 Hz to 3000 Hz while the experimental method shows damped vibration frequencies from 500 Hz to 2000Hz. The difference between simulation and experimental results is due to different methods used for generating damped vibration frequencies and demodulation techniques.

Acknowledgements

I would like to express my sincere gratitude towards Dr. BanmaliRawatfor his constant encouragement and valuable guidance during the completion of thesis work.

I would like to thank Dr. Aaron Covington (Department of Physics, University of Nevada, Reno) and Dr.XiaoshanZhu (Department of Electrical and Biomedical, University of Nevada, Reno) for agreeing to be my thesis committee members for my thesis.

I also thank Syam Challa, a Ph.D student in Optical Communication area for helping me through my experimental work. I would also like to thank my friends Anupama Bhat, Juhi Huda and Nikhil Mantrawadi for their moral support and help during my thesis work. Finally I would like to thank my parents for understanding, support, patience and encouragement throughout my work.

Table of Contents

1. Introduction……..……01

2. Fiber Optic Sensors for Detection of Vibrations……...…05

2.1 Intensity-Based Vibration Sensor……....……...……..06

2.2 Fabry-Perot Interferometers Vibration Sensors……..……...……10

2.3 Fiber Bragg Grating Vibration Sensors……...……14

3. Basic Theory Analysis…….20

3.1 Damped Vibration and its importance…….....20

3.2 Rayleigh Backscattering Continuous and Damped Vibration Sensor……...22

3.3 Multilongitudinal mode fiber laser (MLMFL) sensor…….25

3.4 Analysis for damped vibration…….…….28

4. Simulations results for Damped Vibrations……...……...33

5. Experimental Results..……....…….48

5.1 Experimental Setup……...…….48

5.2 Experimental Results…….....51

6. Conclusion……57

References…….59

List of Figures

Figure 2.1: Classification based on working principle……6

Figure 2.2: Evolution of Intensity based vibration sensor [5]…….6

Figure 2.3: Schematic of working principle of intensity based sensor……7

Figure 2.4: Schematic for microbend senor structure…...……..8

Figure 2.5: Experimental setup used by Pandey and Yadav……9

Figure 2.6: Schematic of sensor used by Perrone and Vallan……..9

Figure 2.7: Publications in Fabry-Perot Interferometer vibration Sensors [28].……...10

Figure 2.8: Schematic of a reflective EFPI sensor connected with one fiber end and measurement system……..11

Figure 2.9: Schematic diagram of dual-cavity fiber Fabry-Perot interferometer for vibration analysis……...12

Figure 2.10: Schematic for In-Fiber Fabry-Perot Interferometric sensor for vibration detection…….13

Figure 2.11: Schematic diagram of in-fiber FPI proposed by Jesus M. Corres et.al…….14

Figure 2.12: (a) Schematic structure of Fiber bragg grating along with periodic variation in core refractive index. (b) Fiber bragg grating reflected power as a function of wavelength [21]…….15

Figure 2.13: Publications in Fiber Bragg grating vibration sensor [35]..…..……16

Figure 2.14: Strain and vibration measurement using FBG sensor……...17

Figure 2.15: Experimental setup for dynamic strain with single fiber proposed by A.Cusano et.al……18

Figure 3.1: System behavior for different zeta (ξ) values……..21

Figure 3.2: Experimental setup to detect continuous and damped vibration by (a) transmitted light (b) Rayleigh Backscattering……...23

Figure 3.3: Schematic of MLMFL sensor……..25

Figure 3.4: Beat frequencies generated between any two modes……..26

Figure 3.5 Mass-Spring-Damper model……28

Figure 4.1: Beat frequencies generated w.r.t change in no. of modes (N)…….33

Figure 4.2: Beat frequencies w.r.t change in cavity length……34

Figure 4.3: Beat frequencies w.r.t change in effective refractive index (η)….……35

Figure 4.4 Mass-Spring Damper model…….36

Figure 4.5: Damped vibration frequencies generated w.r.t. spring stiffness (k)……37

Figure 4.6: Change in ξ with change in spring stiffness (k)……...……37

Figure 4.7: Amplitude of damped vibrations w.r.t. change in spring stiffness (k)……38

Figure 4.8: Damped vibration frequencies generated w.r.t. damping coefficient (c)……39

Figure 4.9: Change in ξ with change in damping coefficient (c)……...39

Figure 4.10: Amplitude of damped vibrations w.r.t. change in damping coefficient (c)...40

Figure 4.11: Damped vibration frequencies generated w.r.t. mass (m)…….41

Figure 4.12: Change in ξ with change in mass (m)……41

Figure 4.13: Amplitude of damped vibrations w.r.t. change in mass (m)…….42

Figure 4.14 FM Demodulation technique to detect vibration signals……42

Figure 4.15: Downconversion of FM signal……..43

Figure 4.16: Detected damped vibration signals……43

Figure 4.17: Damped vibration frequency (Hz) v/s attenuation (dB)……47

Figure 5.1: Schematic of experimental setup……49

Figure 5.2: Experimental setup in Lab……...50

Figure 5.3: Schematic of generation of damped vibrations……...50

Figure 5.4: Average of loss in signal (dB) for different displacements and damped vibration frequencies at time T1..…….52

Figure 5.5: Average of loss in signal (dB) for different displacements and damped vibration frequencies at time T2...……...…….53

Figure 5.6: Average of loss in signal (dB) for different displacements and damped vibration frequencies at time T3...……...…..53

Figure 5.7: Damped vibration frequency (Hz) v/s attenuation (dB)……...…….….52

Figure 5.8: Comparison between experimental and simulation results…….55

List of Table

Table 4.1: Amplitude of output signal for input damped vibrations……..45

Table 5.1: Attenuation of signals (dB) for various damped frequencies……...49

Chapter-1

Introduction

For more than 20 years there has been a tremendous growth of optoelectronics and fiber optic communication industries. The optoelectronic industry has developed the products such as laser printer, bar code scanners, compact disc players etc. The fiber optic communication (FOC) industry, on the other hand, has shown progress in telecommunication links by providing higher performance, reliability and bandwidth. The Fiber optic sensor industry has emerged as a major user of technology associated with optoelectronics and FOC. The capability of measurement systems has been greatly enhanced by the use offiber optic sensors which have replaced the traditional sensors such as electrical and mechanical sensors. Sensor applications include rotation, acceleration, pressure, vibration, acoustics, linear and angular position, strain, chemical and viscosity measurements. The advantages of the fiber optic sensor includes: 1) lightweight; 2) small sensing area; 3) high sensitivity; 4) high bandwidth; 5) immunity to electromagnetic interference and 6) environmental ruggedness [1].

Fiber Optic Sensors are classified as follows:

1. **Extrinsic Fiber Optic Sensors:** In an extrinsic fiber optic sensor the sensing takes place in the region outside the fiber. The light travels through the fiber, reaches the sensing region and then this modulated light again travels through fiber for further processing. The extrinsic fiber optics sensors are also known as hybrid fiber optic sensors. In hybrid fiber optic sensor the fiber is used to

carry light to a box where data is collected. The term Extrinsic fiber optic sensor and hybrid fiber optic sensors are used interchangeably.

2. **Intrinsic Optic Sensor:** In these sensors the sensing takes place within the fiber itself and hence the name "intrinsic". The intrinsic fiber optic sensors are also known as "all-fiber" optic sensors [2].

Another subclass of intrinsic fiber optic sensors is interferometric fiber sensors. These sensors fall into a high-performance group and can be used to design Fiber Optic Gyroscopes (which are currently being used in the Boeing 767 class of airplanes). These sensors are also used to develop navigational tools by some auto makers like Honda, Volvo, and BMW etc. Interferometric Fiber sensors are also used in the manufacturing of Hydrogen detectors.

The fiber optic sensors technology is evolving and improving each day. The fiber sensors offer improved performance, reliability, safety, and cost advantage to users. This has led to the fiber optic sensors being used as a direct replacement for existing traditional sensors. The successive development of fiber optic sensors in the area of fiber optic gyro is replacing both mechanical and laser ring gyros for medium accuracy devices. In the United States rapid developments are being made in fiber optic sensor technology to support the application such as Fly-by-light [3]. The fiber optic sensors are also being incorporated in manufacturing and medical fields.

In the medical industry, fiber optic sensors are completely passive in its sensing operation. They are used for blood-gas measurement as they pose no electric-shock threat to the patients [4]. The other industries which are taking a keen interest in optical sensors

are the automotive and construction industries. Along with a fiber optic communication link, fiber optic sensors can be used to monitor stress buildup in critical fault locations and dome buildup of volcanoes [5].

Fiber optic vibration sensorsare used to monitor structural faults in hydroelectric dams, mechanical vibrations at power transformers and vibrations due to earthquakes [6-8]. Some of the techniques that have been proposed for detection of vibrations are Fabry-Perot interferometric, Bragg grating [9-12] sensors. As the demodulation method used in these systems is in optical domain, which leads to problems like complexity of the method used, instability of the sensing system and high costs of the system. In order to simplify the sensing system and make it less complex, a new method of sensing has been proposed. The concept is based on the multilongitudinal fiber ring laser sensor [13]. In this sensor the laser cavity is formed using single mode fiber (SMF), an erbium doped fiber (EDF), fiber bragg grating (FBG) and 3dB coupler. The multilongitudinal modes are produced in the cavity when it is pumped with a 980 nm source. The beat frequencies are produced by beating any two modes in the cavity. This acts as a carrier frequency for vibration signal acting as a modulating signal. Thus this frequency modulated signal from the sensor is detected by a photodiode (PD) and then it is filtered and demodulated.

This thesis aims at the detection of damped vibrations signals using beat frequency and the frequency modulation-demodulation technique. The thesis is outlined into the following chapters. Chapter two presents details about the different sensor techniques used to detect vibrations. Chapter three focuses on basic theory and analysis for signal output from sensor. Chapter four focuses on simulation for detection of damped

vibrations. Chapter five discusses about the experimental results. Finally, chapter six concludes the research conducted and discusses future scope of the subject area.

Chapter-2

Fiber Optic Sensors for Detection of Vibrations

The traditional sensors like capacitive and piezoelectric accelerometers have been used for maintenance of heavy electromechanical equipment in the past. The electromagnetic interference (EMI) can be troublesome when electric signals are used in noisy conditions (e.g. power plant generators with high EMI) to detect and transmit relevant physical parameters. Over the past decade fiber optic sensors has expanded into fiber optic telecommunications with the growth of optoelectronic devices [14-16]. New technologies that are evolving due to advancements in fiber optic sensors have enabled the vibration monitoring for heavy electric machinery. Due to advantages listed in Chapter 1 the use of fiber optic sensors are increasing daily. Moreover fiber optic sensors give perturbation free means of monitoring vibration in the presence of electromechanical equipment.

The classifications of fiber optic sensors are done in two groups: 1. Extrinsic: the sensing is done outside the fiber and 2. Intrinsic: the sensing is done within the fiber itself [17]. More details about the classifications are discussed in chapter 1. The different methods for vibration detection based on their working principle are shown in Figure 2.1.

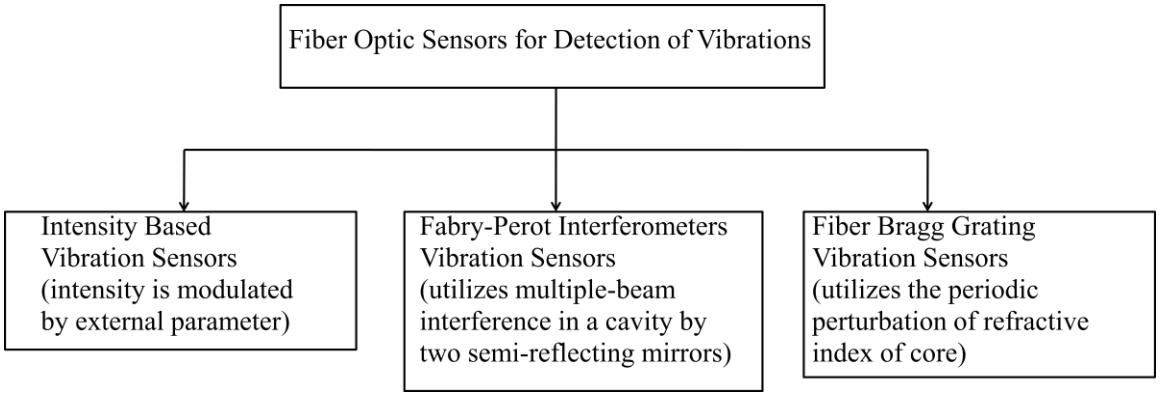

Figure 2.1: Classification based on working principle.

2.1 Intensity-Based Vibration Sensor

The study of intensity based sensors for detection of vibrations has been done for more than 25 years. Figure 2.2 shows the statistical growth of these sensors.

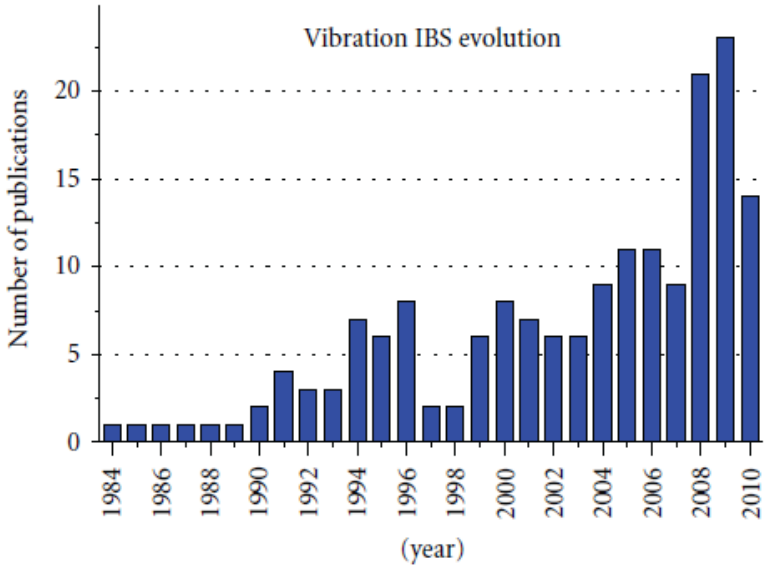

Figure 2.2: Evolution of Intensity based sensor [5].

As seen from Figure 2.2 the most of the development work of intensity based sensors for detection of vibrations started in the year 2008-2009. In the intensity-based sensor the light intensity from a source is modulated by the measurand and then is guided through fiber to the detector. Further this detected signal is processed using signal processing system. Figure 2.3 shows the schematic of the working principle of intensity based senor.

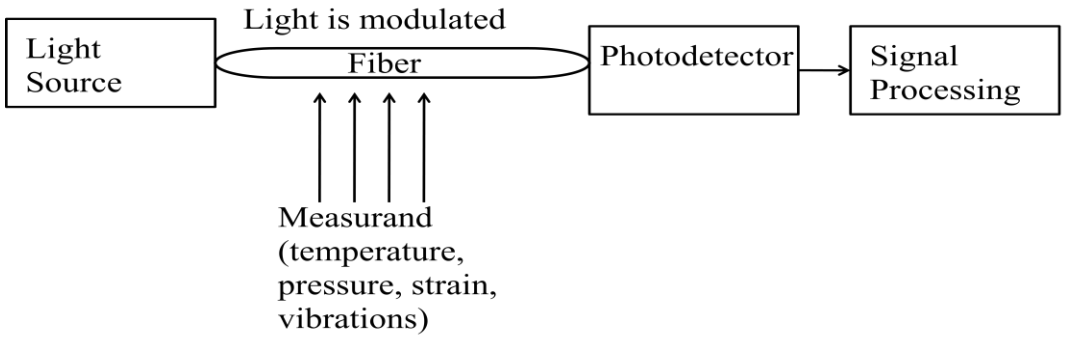

Figure 2.3: Schematic of the working principle of intensity based sensor.

Intensity based vibration sensors can be classified as contact or noncontact sensors. In a noncontact vibration sensor the signal is reflected from the vibrating surface and then detected by the sensing fiber. Conversely, a contact vibration sensor uses the transmissiveproperty of the fiber. The first intensity-based sensors developed were microbend sensors [19-21]. The working principle of microbend structure is that the transmitted power is changed w.r.t. to some physical parameters (vibration, pressure, strain, etc.). Figure 2.4 shows a schematic for a typical microbend fiber optic sensor. In Figure 2.4, the light intensity fluctuates due to microbends caused by vibrations and the intensityvariation of light is monitoredby a detector.

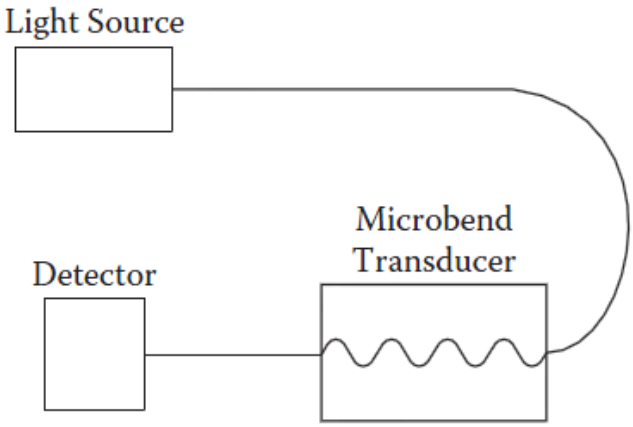

Figure 2.4: Schematic for microbend senor structure.

The fiber deformation affects the coupling of optical power from core guided modes to higher order radiating modes. These modes are attenuated by the surrounding medium. For microbend sensor both multimode and single mode fiber has been used [22-24]. The maximum sensitivity is achieved when the bending frequency is equal to the difference between propagation constant of the propagating modes and radiation modes in a multimode fiber,as investigated by John W. Berthold III.M.Kuhn has investigateda single mode fiber optic microbend sensor where maximum sensitivity is achieved when the spatial bend frequency is equal to difference between propagation constant of fundamental mode and a discrete cladding mode [25].

Pandey and Yadav have proposed intensity based sensor technique for high pressure and crack detection as shown in Figure 2.5 [26]. They have developed the sensor to detect cracks and pressure in construction panels, where change in optical power was directly proportional to the applied pressure at the sensor.

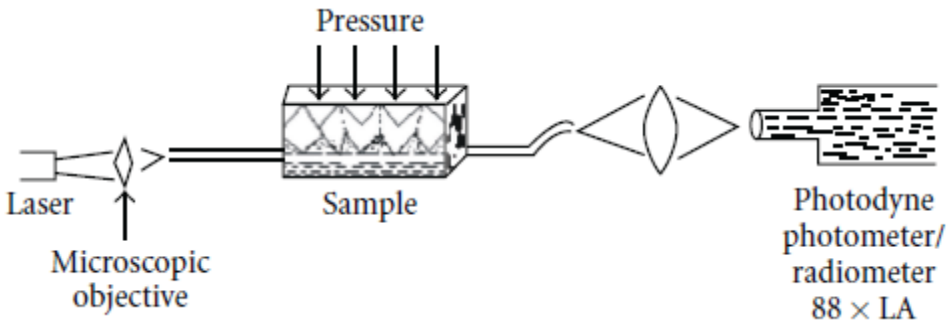

Figure 2.5: Experimental setup used by Pandey and Yadav.

Commonly used intensity-based sensor for vibration detection is noncontact displacement intensity-based sensor. In non contact intensity based senor, one fiber is used to send the light pulse to the reflecting surface of the target and another fiber is used to detect that reflected light. This technique was proposed by Guido Perrone and Alberto Vallanas shown in Figure 2.6 [27]. They have tested the system for different reflecting target surfaces (like loudspeaker and electrodynamic shaker).

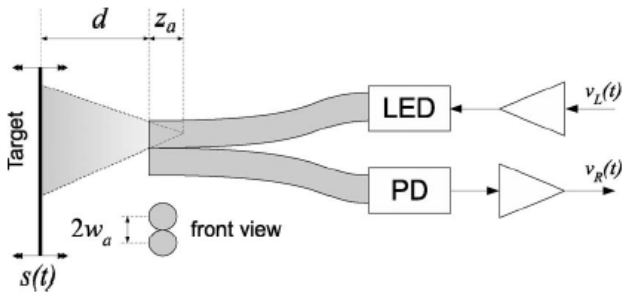

Figure 2.6: Schematic of sensor used by Perrone and Vallan.

They have used plastic optical fiber (POF's) as a sensing head and simple spectral analysis for analyzing the amplitude of vibration signal. Thus they have shown that their system can measure the amplitude of the vibration up to 40 kHz with 1μm of resolution.

In intensity based sensors, optical power can fluctuate due to variation in sources, connector, couplers used in the sensor system which introduces error in the output signal. Without the referencing mechanism the output signal cannot be accurately calibrated and would result in errors. Thus for intensity based vibration senor, in many cases it requires referencing mechanism to calibrate the sensor output.

2.2 Fabry-Perot Interferometers Vibration Sensors

Fabry-Perot interferometers (FPI) are constructed by placing two semi-reflecting mirrors separated by length L, to form acavity where the optical beam interfers due to multiple reflections. Figure 2.7 shows the growth of publications and interest in FPI vibration sensors, indicating that main growth took place after 2004. In order to use FPI as a sensor partial mirrors are to be created inside the fiber. This can be done using chemical or fusion current processes. FPI can be classified as extrinsic FPI and In-fiber FPI.

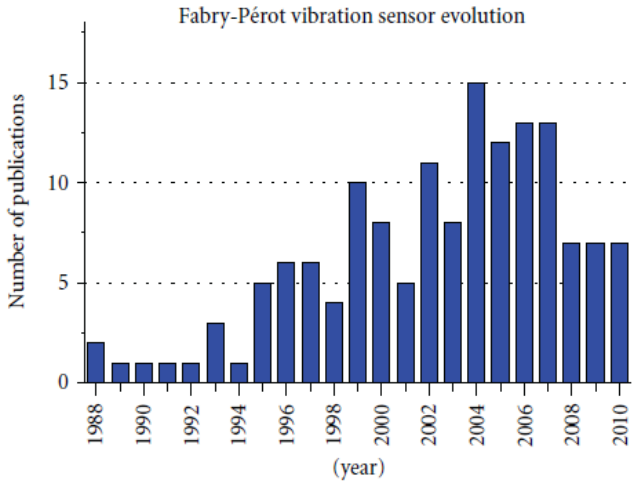

Figure 2.7: Publications in Fabry-Perot Interferometer Vibration Sensors [28].

Sudarshan and Claus were the first to propose extrinsic Fabry-Perot interferometer (EFPI) sensor [29]. In their proposed method the optical cavity is external to the fiber. Gangopadhayay et.al. showed in their paper that EFPI can be used for vibration measurement as shown in Figure 2.8 [30].

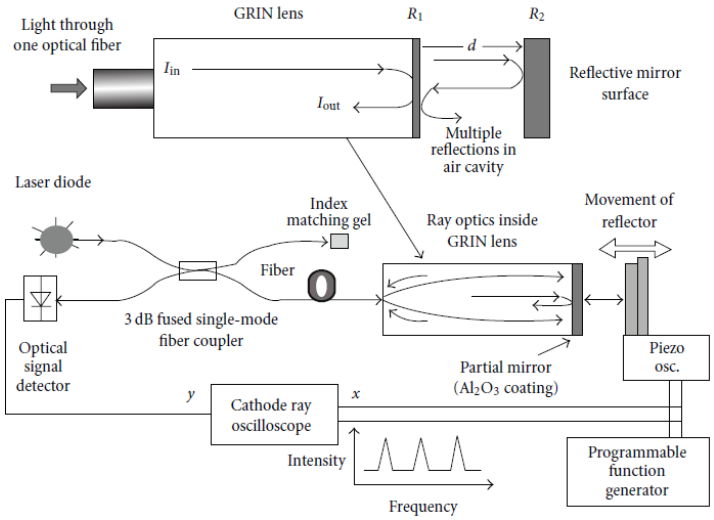

Figure 2.8: Schematic of a reflective EFPI sensor connected with one fiber end and measurement system.

In this method the wavelength transform (WT) was used for counting the optical fringes in the sensor output signal. The WT method was used to identify the frequency component from non-sinusoidal vibration signal of multiple fringes and complex frequency measurements. This system is flexible, better sensitivity and provides real-time measurements of surface vibrations. The EFPI along with fiber optic data transmission can be used in harsh environmental conditions. As per the principle of Fabry Perot model, there are constructive and destructive interference of light due to multiple reflections resulting into fringes. Thus many FPI sensor face the problem of directional ambiguity in

fringe motion as and when the measured target change its direction. To overcome this problem another FPI senor was proposed by Pullteap et.al. to detect vibrations [31]. They have proposed modified fringe counting technique applied to dual cavity fiber Fabry-Perot vibration meter as shown in Figure 2.9.

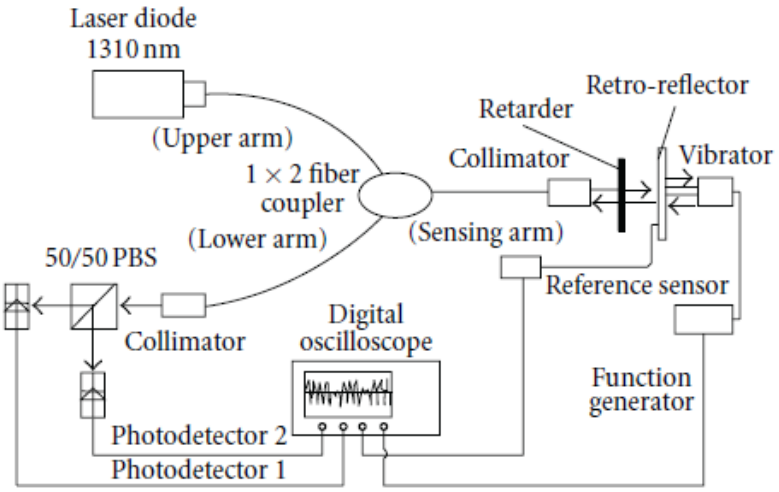

Figure 2.9: Schematic diagram of dual-cavity fiber Fabry-Perot interferometer for vibration analysis.

The advantage of this system is high resolution obtained without using any complicated signal processing system.

Yoshino was the first to implement application of in-fiber Fabry-Perot interferometer (IFFPI) as shown in Figure 2.10 [32]. He proposed the single mode fiber FPI for impact vibrations with 70% end-reflectance.

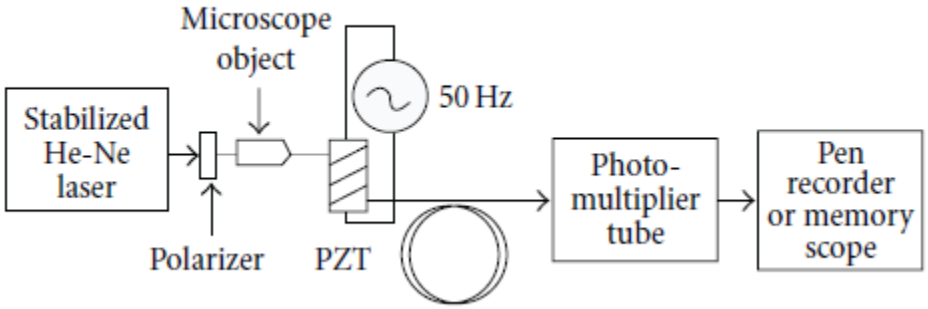

Figure 2.10: Schematic for In-Fiber Fabry-Perot Interferometric sensor for vibration detection.

The output from the sensor was obtained as a change in optical fringes with applied mechanical vibrations. The other application developed using FPI was proposed by Jesus M. Correset.al. as shown in Figure 2.11 [33]. They used this method to detect vibration produced from three phase motor under unbalanced conditions. They have shown the relation between reflected optical power and cavity deformation in the equation given by

$$R_{DH} = A * \left[1 + V * cos \frac{4\pi * L * \varepsilon}{\lambda}\right] \qquad (2.1)$$

where A and V are constants representing amplitude and visibility of sensor, respectively, λ is wavelength of optical source, L is length of cavity, and ε is deformation of cavity.

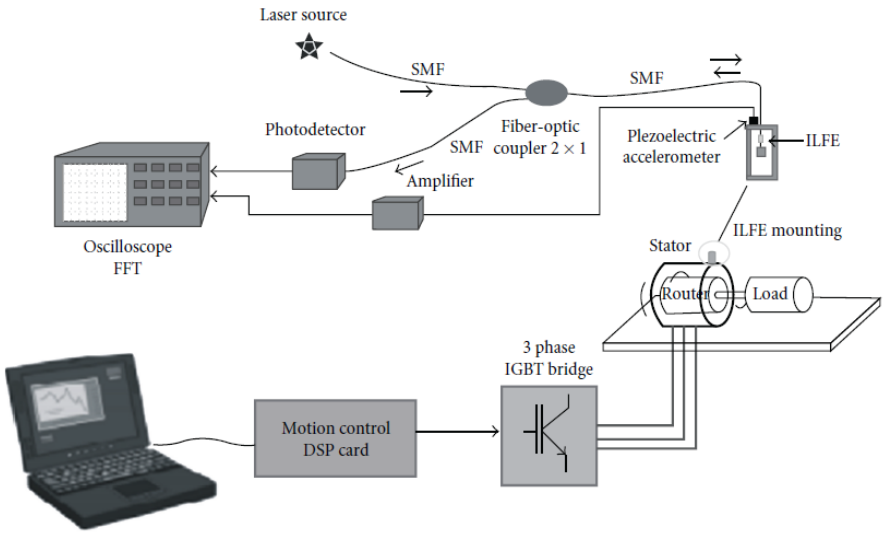

Figure 2.11: Schematic diagram of in-fiber FPI proposed by Jesus M. Corres et.al.

For measuring real time vibrations FPI shows a high precision performance. The FPI sensors are one of the most sensitive systems in fiber optic sensors. The drawback of FPI is the imperfection and misalignment of mirrors, which affects the accuracy of the system.

2.3 Fiber Bragg Grating Vibration Sensors

The Fiber Bragg Gratings (FBGs) have periodic perturbations of refractive index of core resulting in Fresnel reflections. Bragg gratings are created by inscribing the periodic variation of refractive index into the core of fiber. The light travel through these periodic grating of core refractive indices reflect and refract at the interface. Figures 2.12 (a) and (b) shows the schematic structure of fiber bragg gratings and reflected power as a function of wavelength, respectively.

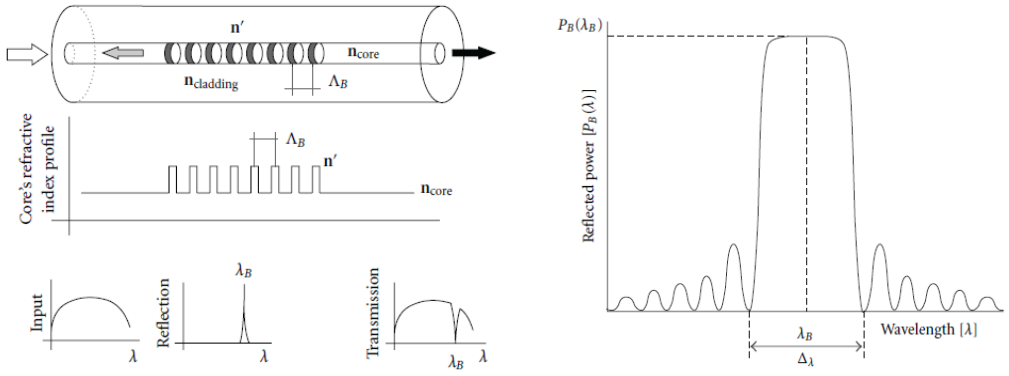

(a) (b)

Figure 2.12: (a) Schematic structure of Fiber bragg grating along with periodic variation in core refractive index. (b) Fiber bragg grating reflected power as a function of wavelength [34].

The wavelength spacing between the first maxima or bandwidth ($\Delta\lambda$) is given by

$$(\Delta\lambda) = (2\ \delta\eta_0\eta/\pi)\ \lambda_B \qquad (2.2)$$

where, $\delta\eta_0$ is variation is refractive index (η'- η_{core}) (refer Figure 2.12 (a)), η is fraction of power in the core and λ_B is reflected wavelength. Figure 2.13 shows the publication in FBG sensor, indicating that the growth took place after 2006.

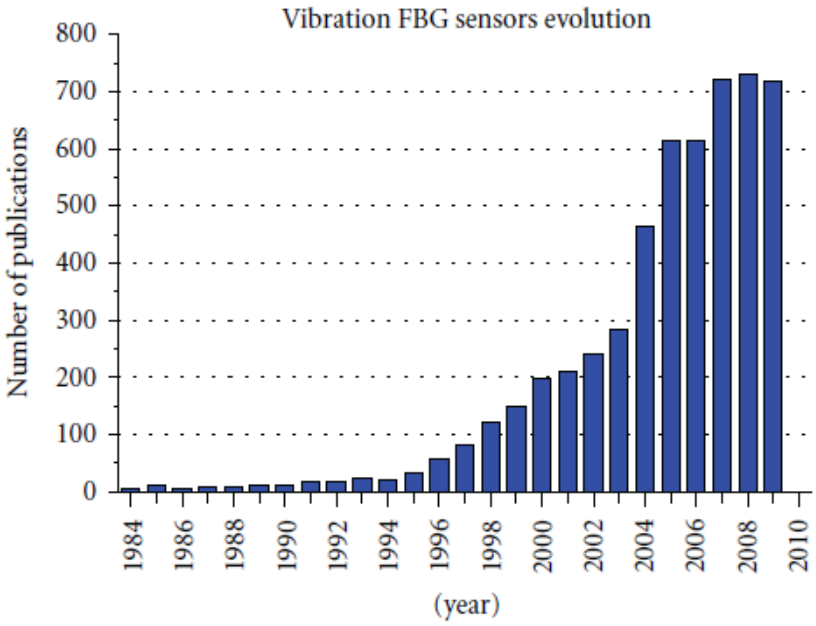

Figure 2.13: Publications in Fiber Bragg grating vibration sensor [35].

One of the properties of FBG is their dependence on the resonance peak at very small variation of Bragg period,which makes suitable for stain measurements [36-37]. Also due to these applied pressure and temperature the grating period and photoelasticity is changed which in turn changes the Bragg wavelength. High speed dynamic strain variations are seen due to vibrations. In measuring these dynamic strains a sensitive monitoring system is required to measure the position of resonance FBG wavelength. In order to achieve this, system performance slows down. M. A. Davis and A. D. Kersey proposed a method to overcome this problem shown in Figure 2.14 [38].

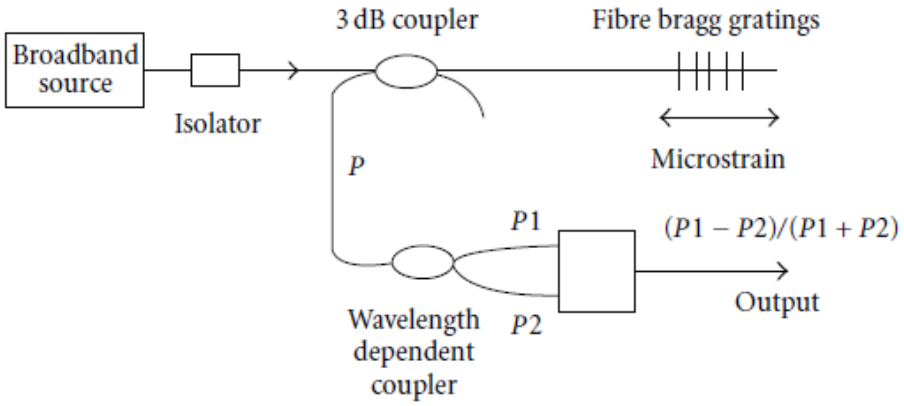

Figure 2.14: Strain and vibration measurement using FBG sensor.

In this method, to achieve high speed detection two or more different wavelength components of reflected light from FBG are splitted and combined with conventional intensity based optoelectronic detector. The reflected light from FBG is sent to wavelength dependent coupler through a 3dB coupler. The output from wavelength dependent coupler will vary in intensity as the reflectivity of FBG is changed due to the applied strain. To measure this output simple signal processing can be used to know the voltage which is directly proportional to strain. Another approach for measurement of dynamic strain was proposed by A. Cusano et.al. as shown inFigure 2.15 [39]. In their method the reflected light from FBG is divided by optical filter to match the Bragg wavelength.The reflected light is divided into two components by an optical filter. Thus when the Bragg peak is changed due to applied strain the two components vary in their relation with respect to each other. Because of passive arrangement of demodulation system the vibrations that are measured with this system are up to 400 kHz. The sensitivity of their system is limited by the electronic measuring stage. For measurement of vibration the bandwidth of the system limits the application range of the system.

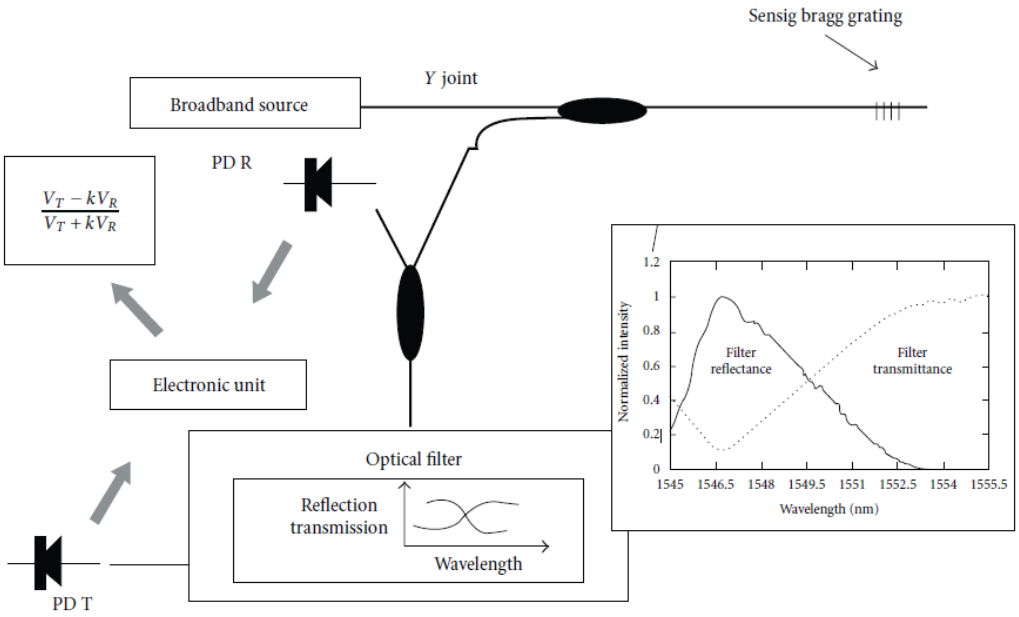

Figure 2.15: Experimental setup for dynamic strain with single fiber proposed by A.Cusano et.al.

FBGs used as seismic sensorwas investigated by A. Laudati et.al. [40]. They used three different Bragg sensors which are simultaneously compared with the conventional accelerometer. It gives high sensitivity for dynamic stain (vibrations) and has an extended dynamic response.Due to the added advantage of small size of FBG sensors, they are used to embed into composite material and concrete [41-42]. Due to its multipoint sensing capability it is used in civil structures like bridges and highways [43-44].

This chapter reviews about different methods used for the vibration detection. First method proposed for vibration detection was intensity-based senor. This can be used in reflection and transmission mode as explained in section 2.1. But this technique is dependent on high accuracy of the source power level. The Fabry-Perot interferometer has high resolution and accuracy. But the system is expensive as explained in 2.2. Fiber

Bragg Grating method provides unique accuracy and wavelength multiplexing capability for several sensing points. However in this method detection is done in optical domain using optical filter or optical interferometer. This makes system more complex and expensive. Fiber optic sensors are highly durable and economical for vibration measurement, thus increasing the scope of applications and new research fields.

Chapter-3

Basic Theory and Analysis

3.1 Damped Vibration and its importance

Mechanical Vibration is a phenomenon which is periodic and repetitive. Damping is the mechanical phenomenon by which mechanical energy is dissipated in mechanical systems [45]. In damping the amplitude of oscillations gradually decreases with time. Damped harmonic oscillator generally satisfies the second order differential equation given as

$$\frac{d^2x}{dt^2} + 2\xi\omega_o \frac{dx}{dt} + {\omega_0}^2 x \tag{3.1}$$

where, ω_0 is undamped angular frequency and ξ is damping ratio [46].

With respect to the value of damping ratio ξ the behavior of the oscillatory system can be classified as follows:

1. **Overdamped system:** The oscillatory system is said to be over damped when ξ>1. In overdamping the system comes to equilibrium without oscillating. The simple example for overdamped is the shock absorbers in cars. When the car is hit to a bump, the cars acts as an over damped system, because the car settles to its original position immediately.
2. **Critically damped system:** The system is critically damped when ξ=1. The oscillatory system comes to equilibrium as soon as possible without oscillating.

The example of critical damping is when a bullet is fired from a gun; it comes to neutral position in no time. There isn't much difference between overdamped and critically damped system. But critically damped system comes to equilibrium in much less time than overdamped system.

3. **Underdamped system:** The system is said to be underdamped when ξ<1. The oscillatory system comes to its stable state gradually. It means that the amplitude of oscillations reduces gradually. The example of underdamped are cantilever beam and seismic waves. Figure 3.1 shows the system behavior for different zeta (ξ) values.

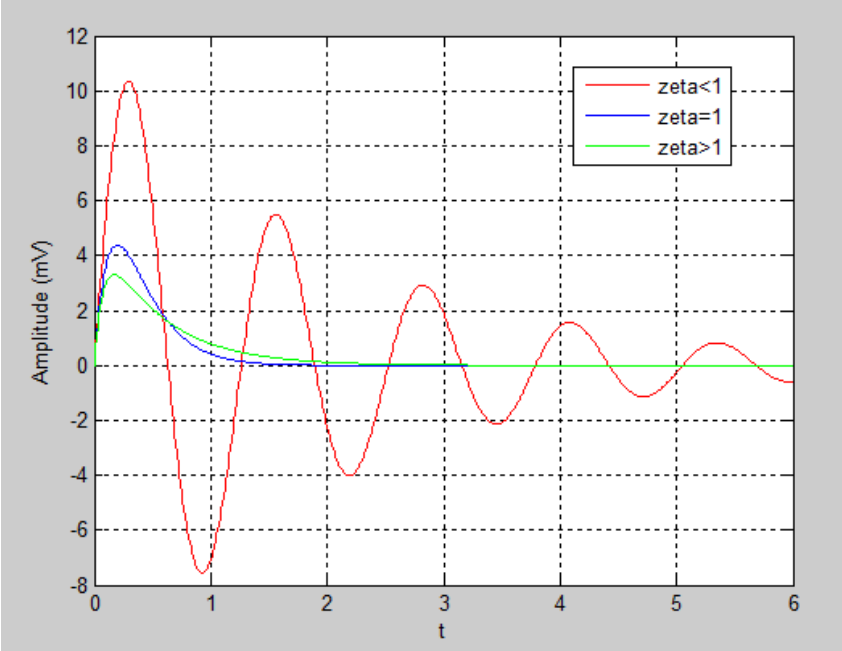

Figure 3.1: System behavior for different zeta (ξ)values.

Different mechanisms used to produce these damped vibrations are cantilever beam, RLC circuit, mass-spring-damper model and piezoelectric accelerometer. In real world

the damped vibration are seen during earthquakes, in heavy electromechanical equipments, structural misalignment in hydroelectric dam, and environmental impact on bridges. Thus to monitor and take the precautionary measures, the damped vibration detection is necessary.

3.2 Rayleigh Backscattering Continuous and Damped Vibration Sensor

ZiyuZang and Xiaoyi Boa have developed the sensor to detect continuous and damped vibrations based on Rayleigh Backscattering [47]. They have proposed the polarization diversity vibration sensor that is used for structural vibrations under external disturbances. This method shows improved signal-to-noise ratio over 13 dB with a capacity to detect the signal up to few kilo-hertz. The signal to noise ratio for this sensor is greater than 37dB combined for both continuous and damped vibrations. The basic principle of this technique is the birefringence property of the single mode fiber. The birefringence of fiber is affected by various parameters like temperature, pressure, strain, etc which changes the phase between two polarization modes. The state of polarization (SOP) of light changes at the fiber end. The vibration signal is detected by measuring the difference between the power output of these polarized light in time and frequency domain. The experimental setup used for this method is shown in Figure 3.2. As seen Figure 3.2 (a) and (b) they have used two setups to detect vibrations. One is using transmitted light and another with Rayleigh Backscattering. In their first setup they have used distributed feedback (DFB) laser source. The linearly polarized light from DFB laser is passed through polarization controller and then in to the fiber used for sensing. The polarization beam splitter (PSB) at the end of fiber separates two orthogonally

polarized light beams. The output from the sensor consists of ac and large amount of dc portion. The output from PSB has a phase shift of π. These beams are then detected by a two separate photodetectors, followed by a subtracter to remove dc portion. Since the vibrations are in ac portion of the signal the dc portion is being removed by subtracter.

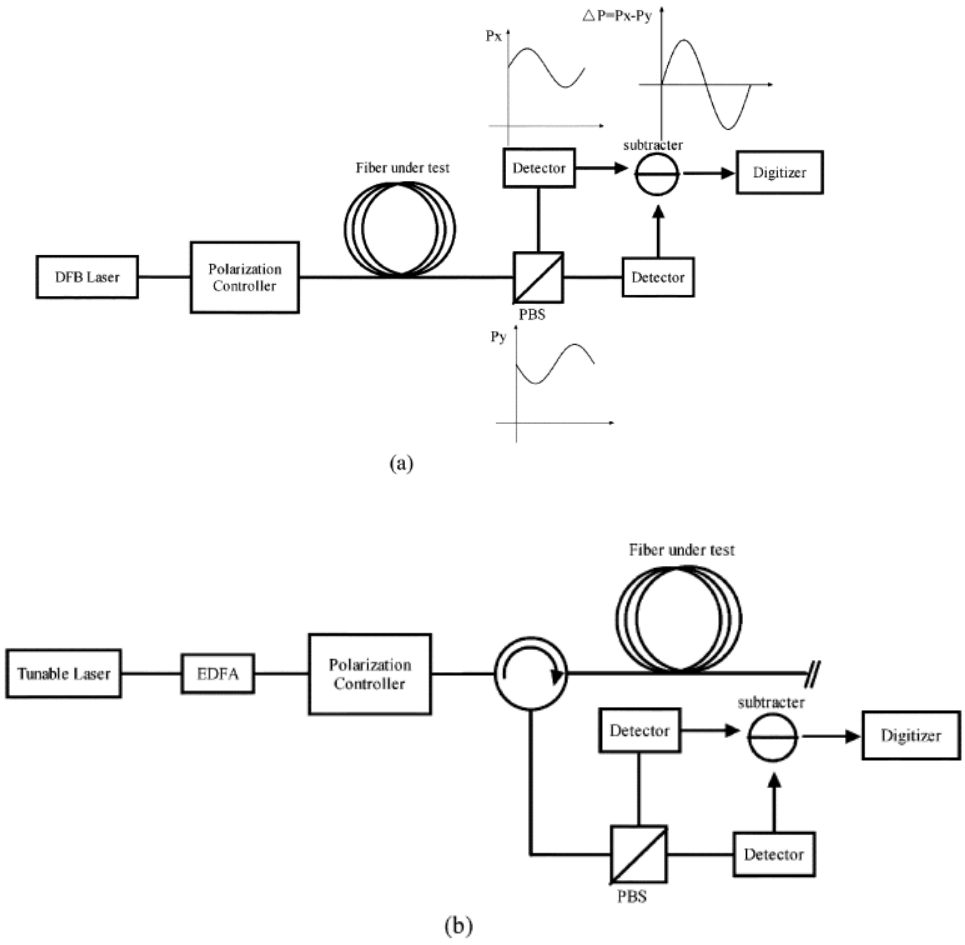

Figure 3.2: Experimental setup to detect continuous and damped vibration by (a) transmitted light (b) Rayleigh Backscattering.

Thus the ac portion which contains vibration signal is been digitized and processed further. For Rayleigh Backscattering, the light beam from tunable laser is amplified using

EDFA and then passed through the fiber used for sensing. For detection of vibration same technique was used as explained for transmitted light setup. They have used a few meter long piezo fiber stretches which produces continuous vibrations and vibrating cantilever for generating damped vibrations. Using this polarized based optical sensor they have measured the vibrations upto16kHz.

The shortcoming of the method is the instability of the system because the demodulation is done in optical domain. Since demodulation of output signal from sensor is done is optical domain the system become complex and expensive. Due to birefringence there is a phase shift between two polarized modes. They measure the power change in these polarized lights to detect the vibration signal. But the birefringence will also be affected by other environmental conditions such as temperature and pressure. So this system will require temperature compensation circuitry and pressure calibration system to detect vibration signals. This method also needs an end reflection compensation system. Tiny loops are to be made at end of the sensing fiber to avoid these end-reflections due to bending loss.

A new method is proposed based on beat frequency and frequency modulation-demodulation technique which is simple and low-cost. This method is based on the principle of multilongitudinal mode fiber ring laser (MLMFL). The laser cavity in MLMFL is formed using Erbium doped fiber (EDF), Single mode fiber (SMF), Fiber Bragg grating (FBG), and 3dB optical coupler.

3.3 Multilongitudinal mode fiber laser (MLMFL) sensor

The MLMFL method for detection of strain and temperature measurement was proposed by S.Lui et.al. [48-52]. The schematic of MLMFL is shown in Figure 3.3.

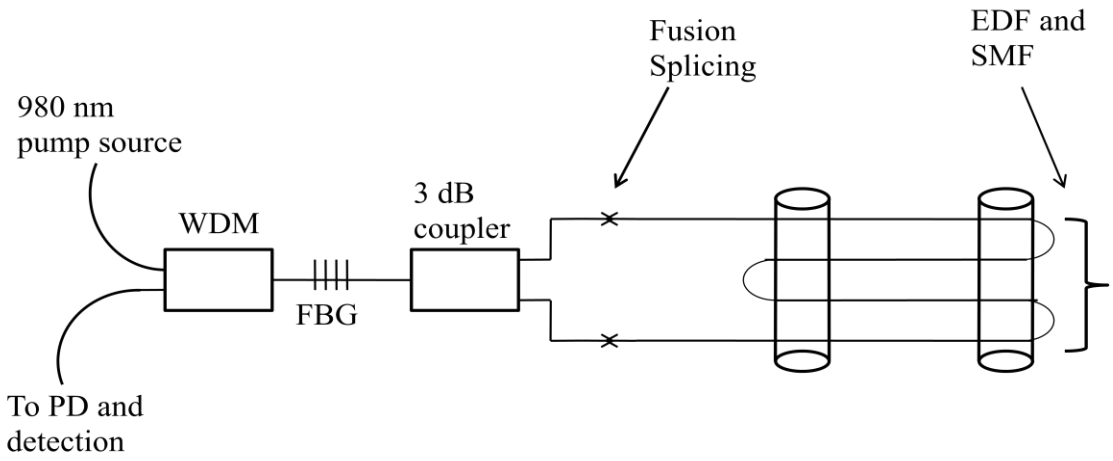

Figure 3.3: Schematic of MLMFL sensor.

As shown in Figure 3.1 the Erbium doped fiber (EDF), Single mode fiber (SMF), Fiber bragg grating (FBG) and a 3-dB coupler forms a ring resonant cavity. The erbium doped fiber (EDF) provides gain for resonant cavity. When the 980 nm pump source power is launched through WDM many longitudinal modes are established within the reflected bandwidth of FBG. Several beat frequencies are produced by beating any two modes in the cavity. The beat frequencies generated in the cavity are shown in Figure 3.4.

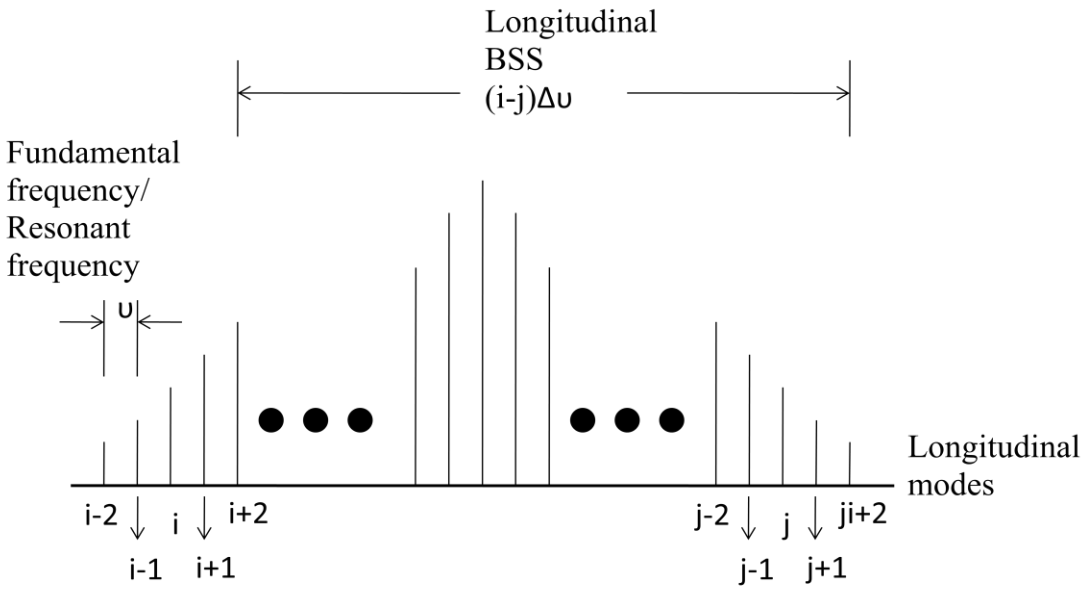

Figure 3.4: Beat frequencies generated between any two modes.

The beat frequency is given as,

$$f_N = \frac{c}{\lambda_i} - \frac{c}{\lambda_j} = \frac{Nc}{2\eta L} \tag{3.2}$$

where, λ_i and λ_j are the wavelengths at i^{th} and j^{th} mode, N is longitudinal laser mode number (N=1, 2, 3, 4 …), c is velocity of light in vacuum ($3*10^8$ m/s), L= length of cavity (meters), η is effective refractive index and f_N is beat frequency.

Fiber experiences strain when the vibrations are applied to the fiber. This strain changes the length of laser cavity and thus the beat frequency f_N. The change in beat frequency is given as [53]

$$df_N = N\, d\left(\frac{c}{\eta L}\right) = -N\left(\frac{c}{\eta L}\right)\left(\frac{d\eta}{\eta} + \frac{dL}{L}\right) \tag{3.3}$$

Therefore the equation (3.2) becomes as,

$$df_N = -f_N(1 - \rho e)\varepsilon \tag{3.4}$$

where, ρe is the strain optic coefficient and ε is the strain experienced by the fiber due to applied vibrations.

As mentioned earlier the fiber experiences strain due to applied vibrations. Since the applied vibrations are continuous the induced strain can be given as,

$$\varepsilon = A_m \cos(2\pi f_m t) \tag{3.5}$$

where, A_m is the amplitude of the strain which is proportional to the acceleration of vibration signal and f_m is the vibration frequency.

Now substitute equation (3.5) into equation (3.4) the change in beat frequency is given as,

$$df_N = (-f_N(1 - \rho e))A_m \cos(2\pi f_m t) \tag{3.6}$$

The modulated beat frequency from the sensor at time t is given as,

$$S_N(t) = a_N \cos\left(2\pi \int \varepsilon(t) dt\right) \tag{3.7}$$

where, aN is output intensity from photodiode (PD) and ε(t) is the strain.

Therefore the final output from sensor is,

$$S_N(t) = a_N \cos\left(2\pi f_N t + 2\pi \int -f_N(1 - \rho e) A_m \cos(2\pi f_m t)\, dt\right) \tag{3.8}$$

Integrating equation (3.8) the sensor output becomes,

$$S_N(t) = a_N \cos\left(2\pi f_N t + \frac{(-f_N(1-\rho e))A_m}{f_m} \sin(2\pi f_m t)\right) \quad (3.9)$$

where, f_N is the carrier frequency and $-f_N(1-\rho e)A_m$ is the maximum frequency deviation.

3.4 Analysis for damped vibration

In real practices all systems are damped for which the energy is dissipated and amplitude gradually reduces until it stops completely. For the analysis of damped vibration we have considered free damped vibrations and forced damped vibration. To generate these damped vibrations we will consider the mass-spring-damper model. Figure 3.5 shows the mass-spring-damper model.

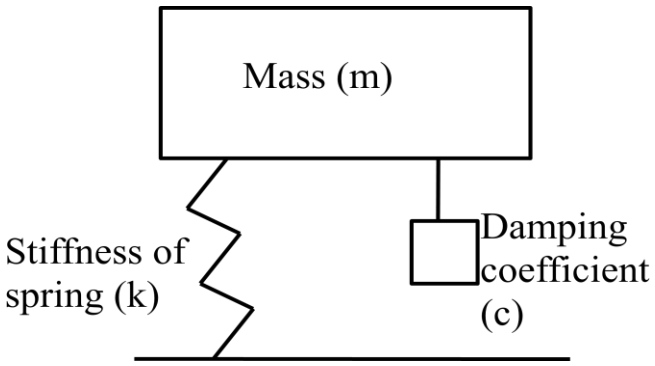

Figure 3.5 Mass-Spring-Damper model.

A. Free Damped Vibrations

In a free damping, the system oscillates when no external force is applied to the system. The output of the damper model shown in Figure 3.5 is a force proportional to the velocity of mass. Therefore the damping coefficient (c) has the unit of force and is given by $F_d = -c_d\frac{dx}{dt}$, where F_d is damping force and c_d is damping coefficient.

Therefore the strain induced on fiber can be given as [54]

$$\varepsilon = X\, e^{-\xi 2\pi f_m t}\cos\left(\sqrt{1-\xi^2}2\pi f_m t - \varphi\right) \tag{3.10}$$

where, ξ is damping ratio and X is the amplitude of vibration signal.

Now the change in beat frequency w.r.t. free damped vibration is obtained by substituting equation (3.10) into equation (3.4) we get,

$$df_N = (-f_N(1-\rho e))X\, e^{-\xi 2\pi f_m t}\cos\left(\sqrt{1-\xi^2}2\pi f_m t - \varphi\right) \tag{3.11}$$

Therefore the signal output from the sensor for applied free damped vibration is,

$$S_N(t) = a_N \cos\Big(2\pi f_N t + \int (-f_N(1-\rho e))X\, e^{-\xi 2\pi f_m t}\cos\left(\sqrt{1-\xi^2}2\pi f_m t - \varphi\right)\Big) \tag{3.12}$$

Integrating equation (3.12) we get,

$$I2=\int (-f_N(1-\rho e))X\, e^{-\xi 2\pi f_m t}\cos\left(\sqrt{1-\xi^2}2\pi f_m t - \varphi\right) \tag{3.13}$$

Applying integral of exponential function to equation (3.13) we get,

$$I2 = \frac{(-f_N(1-\rho e))X}{2\pi f_m} e^{-\xi 2\pi f_m t}\left[\sqrt{1-\xi^2}\sin\left(\sqrt{1-\xi^2}2\pi f_m t-\varphi\right)\right.$$
$$\left.-\xi\cos\left(\sqrt{1-\xi^2}2\pi f_m t-\varphi\right)\right] \quad (3.14)$$

Substitute equation (3.14) in equation (3.12) we get,

$$S_N(t) = a_N\cos\left(2\pi f_N t\right.$$
$$+(-f_N(1$$
$$-\rho e))\frac{X}{2\pi f_m}\left\{e^{-\xi 2\pi f_m t}\left[\sqrt{1-\xi^2}\sin\left(\sqrt{1-\xi^2}2\pi f_m t-\varphi\right)\right.\right.$$
$$\left.\left.-\xi\cos\left(\sqrt{1-\xi^2}2\pi f_m t-\varphi\right)\right]\right\}\Big) \quad (3.15)$$

where, $(-f_N(1-\rho e))\ X/2\pi f_m$ is the maximum deviation frequency and f_N is the carrier frequency.

B. Forced damped vibration

In forced damped vibration external force is applied to the damper model shown in Figure 3.5. Here the system is applied with sinusoidal force. This sinusoidal force is given as $F=F_o*\cos(2\pi ft)$, where F_o is harmonic force and f is harmonic force frequency.

Therefore the strain induced on fiber can be given as,

$$\varepsilon = X\cos(2\pi f_m t-\varphi) \quad (3.16)$$

where X is the amplitude of vibration, given as,

$$X = \frac{F_o}{k} \frac{1}{\sqrt{(1 - r^2)^2 + (2\xi r)^2}} \tag{3.17}$$

with $r=f/f_n$ and $\varphi=\arctan\ (2\xi r/(1-r^2))$. Where r is ratio of harmonic force frequency over undamped natural frequency, φ is phase shift and F_o is the initial force.

The change in the beat frequency w.r.t. forced damped vibration is given by substituting equation (3.16) into equation (3.4),

$$df_N = (-f_N(1 - \rho e))X\cos(2\pi f_m t - \varphi) \tag{3.18}$$

Now the signal output from sensor is,

$$S_N(t) = a_N \cos\left(2\pi f_N t + \int (-f_N(1 - \rho e))X\cos(2\pi f_m t - \varphi)\right) \tag{3.19}$$

Integrate equation (3.19),

$$I1 = \int (-f_N(1 - \rho e))\cos(2\pi f_m t - \varphi)dt$$

$$= -f_N(1 - \rho e) \int (\cos(2\pi f_m t)\cos(\varphi) + \sin(2\pi f_m t)\sin(\varphi))dt$$

$$=-f_N(1 - \rho e)(\cos(\varphi)/2\pi f_m\ \sin(2\pi f_m t) - \sin(\varphi)/2\pi f_m \cos(2\pi f_m t))$$

$$= -f_N(1 - \rho e)\frac{1}{2\pi f_m}(\cos(\varphi)\ \sin(2\pi f_m t) - \sin(\varphi)\cos(2\pi f_m t)) \tag{3.20}$$

Substitute equation (3.20) into (3.19), the signal output is,

$$S_N(t) = a_N \cos\left[2\pi f_N t + \frac{(-f_N(1-\rho e))X}{2\pi f_m}(\cos(\varphi)\ \sin(2\pi f_m t) - \sin(\varphi)\cos(2\pi f_m t))\right] \quad (3.21)$$

where, $(-f_N(1-\rho e))X/2\pi f_m$ is the maximum deviation frequency and f_N is the carrier frequency. The simulation results based on the analysis done in this chapter are shown in chapter 4.

Chapter-4

Simulations Results for Damped Vibrations

The analytical simulations are performed using the equations (3.2), (3.10) and (3.15). The detection of damped vibrations is based on the beat frequency and frequency modulation-demodulation technique. The beat frequencies that are produced in the cavity are given by equation (3.2). Where beat frequencies is changed due to change in length of cavity (L), effective refractive index (η) or number of longitudinal modes (N). The beat frequencies generated in the MLMFL sensor due to change in number of longitudinal modes (N) are shown in Figure 4.1.

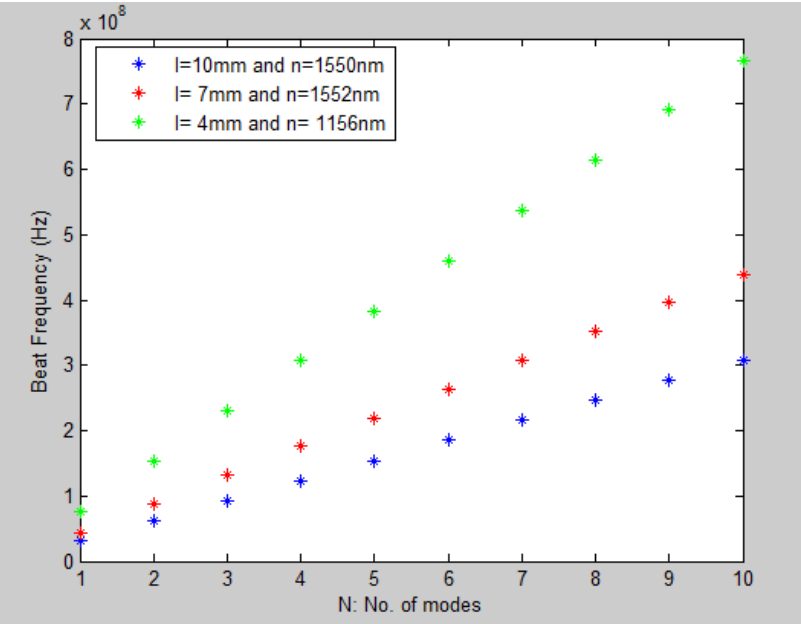

Figure 4.1: Beat frequencies generated w.r.t change in no. of modes (N).

Figure 4.1 shows the change in beat frequencies for 10 longitudinal modes produced in the MLMFL cavity. Change in length of cavity and effective refractive index was kept

constant for three different values. It has been observed that the beat frequencies increase as number of modes increase with a linear relationship (see equation (3.2)). The other parameters that affect the beat frequencies are change in length of cavity (L) and effective refractive (η). Figures 4.2 and 4.3 shows the change is beat frequencies w.r.t change in cavity length (L) and change in effective refractive index (η), respectively.

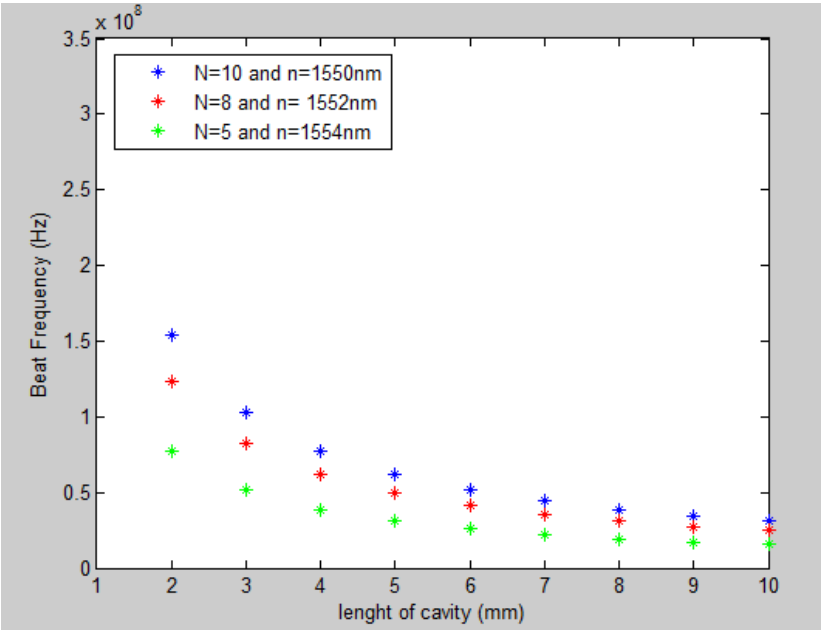

Figure 4.2: Beat frequencies w.r.t change in cavity length.

The change in length of cavity is considered in millimeters, while the change in effective refractive index is considered in step of 0.01. As seen from the Figures 4.2 and 4.3 the beat frequencies decrease as the length of cavity (L) and effective refractive index (η) are increased, respectively. This is observed due to inverse relationship of length of cavity (L) and effective refractive index (η) with beat frequency (see equation (3.2)). But there is not much change in beat frequencies for change in effective refractive index (η). Thus

considering all three parameters the range of beat frequencies generated is from 50MHz to 320MHz.

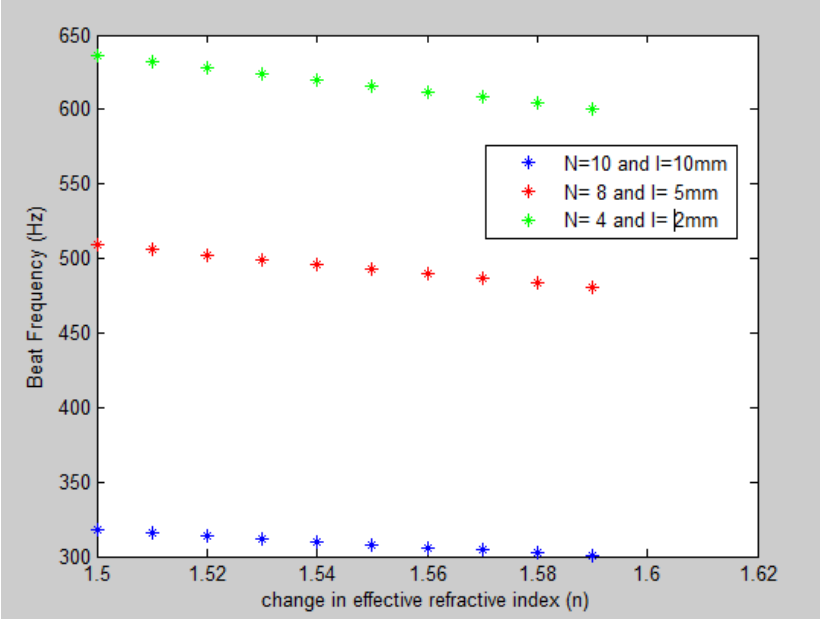

Figure 4.3: Beat frequencies w.r.t change in effective wavelength (η).

In order to generate damped vibration frequency signals the mass-spring damper model is used as shown in Figure 4.4. The differential equation for damped vibration is given by

$$m\ddot{x} + c_d\dot{x} + kx = 0 \qquad (4.1)$$

where, m is a mass, c_d is damping coefficient, k is stiffness of the spring, $\ddot{x}$ and $\dot{x}$ are second and first order derivatives of time, respectively.

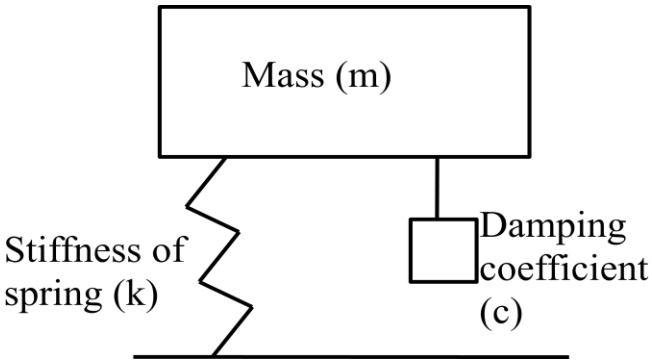

Figure 4.4 Mass-Spring Damper model.

The damped vibration frequencies can be produced by changing spring stiffness (k), damping coefficient (c_d) or mass (m).

A. Changing spring stiffness (k):

Figure 4.5 shows the damped vibration frequencies generated by changing spring stiffness (k) and keeping other parameters constant. It can be seen from the graph that the vibration frequencies increase as spring stiffness is increased. The damping factor zeta (ξ) is given as

$$\xi = \frac{c_d}{2\sqrt{k * m}} \tag{4.2}$$

In order to obtain the damped vibration frequencies the spring constant was varied from 1 to 10. Figure 4.6 shows the change in damping factor ξ w.r.t. spring stiffness (k). The damping factor zeta reduces as spring stiffness is increased (see equation (4.2)). Figure 4.7 shows the amplitude of the frequencies for change in spring stiffness (k). The range of frequencies obtained by changing spring stiffness is from 1000Hz to 3100Hz.

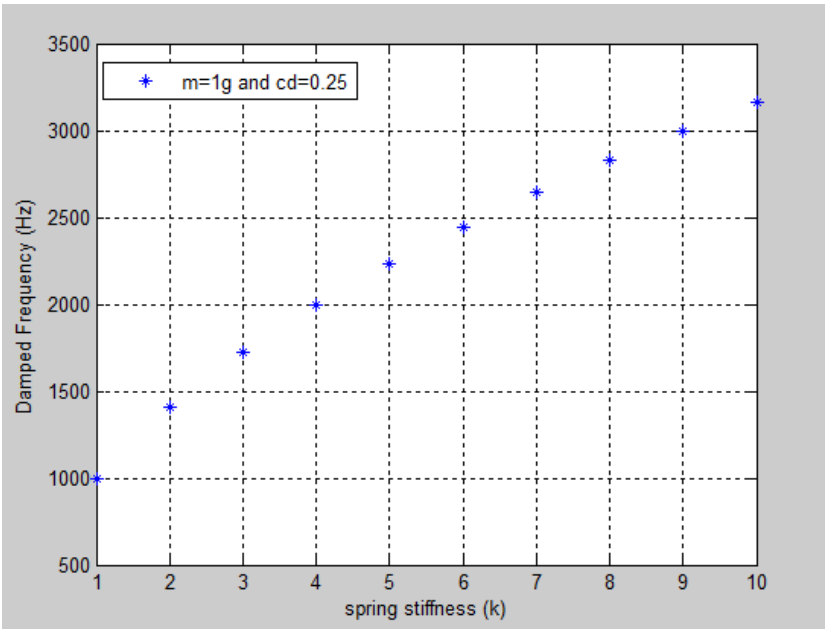

Figure 4.5: Damped vibration frequencies generated w.r.t. spring stiffness (k).

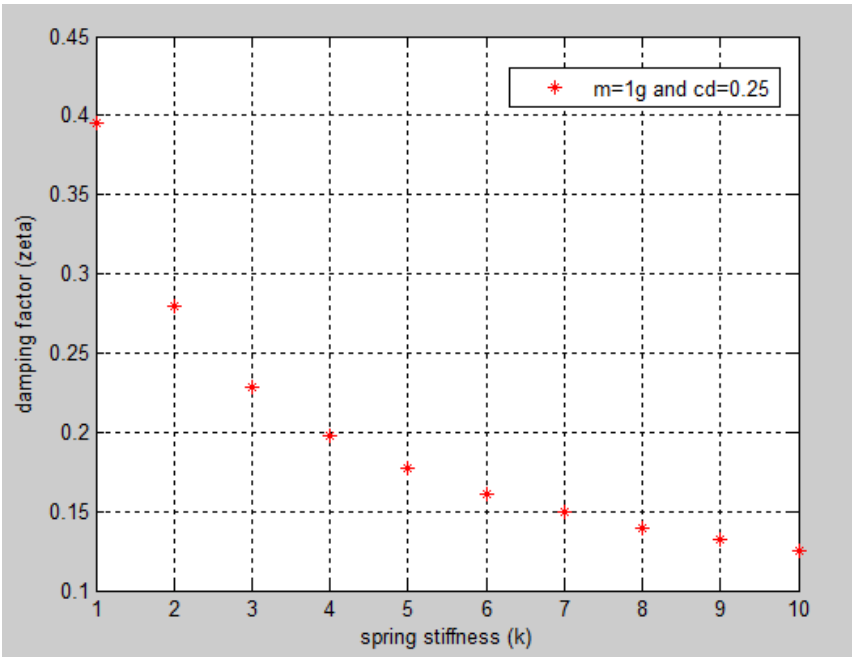

Figure 4.6: Change in ξ with change in spring stiffness (k).

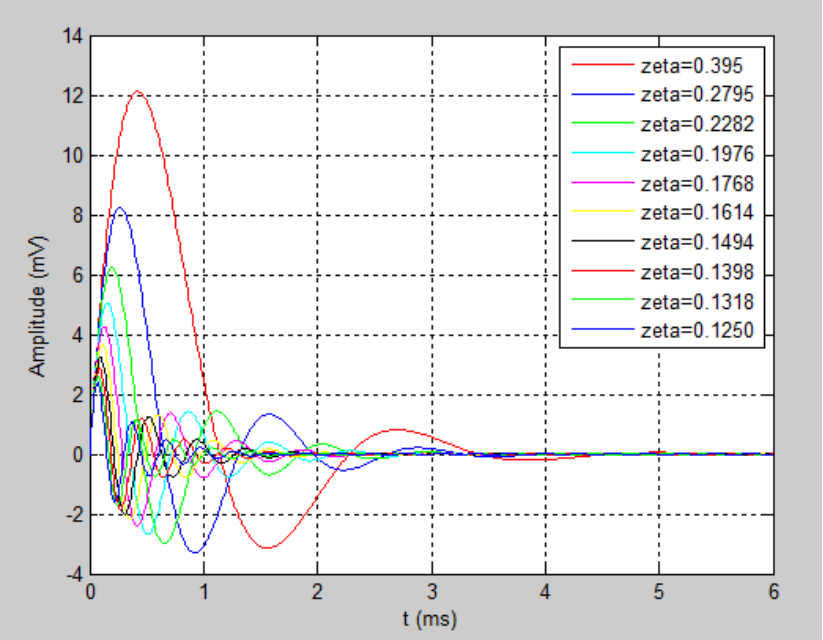

Figure 4.7: Amplitude of damped vibrations.

B. Changing the damping coefficient (c_d):

Now the damped vibration frequencies are obtained by changing the damping coefficient (c_d), while keeping mass and spring stiffness constant. In order generate the damped vibration frequencies the damping coefficient was varied from 0.1 to 1.Figure 4.8 shows the damped frequencies generates w.r.t change in damping coefficient (c_d). As seen from the Figure 4.8 the damped vibration frequencies decrease as damping coefficient (c_d) is increased. While Figure 4.9 shows that zeta (ξ) increase as damping coefficient (c_d) is increased (see equation (4.2)). Figure 4.10 shows the amplitude of the frequencies generated for different values of zeta. The range of frequencies generated with change in damping coefficient (c_d) was very small. It clearly shows that the change in damping coefficient (c_d) does not have much effect on the vibration frequencies. The

range of damped vibration frequencies generated is from 312Hz to 316Hz, which is very small.

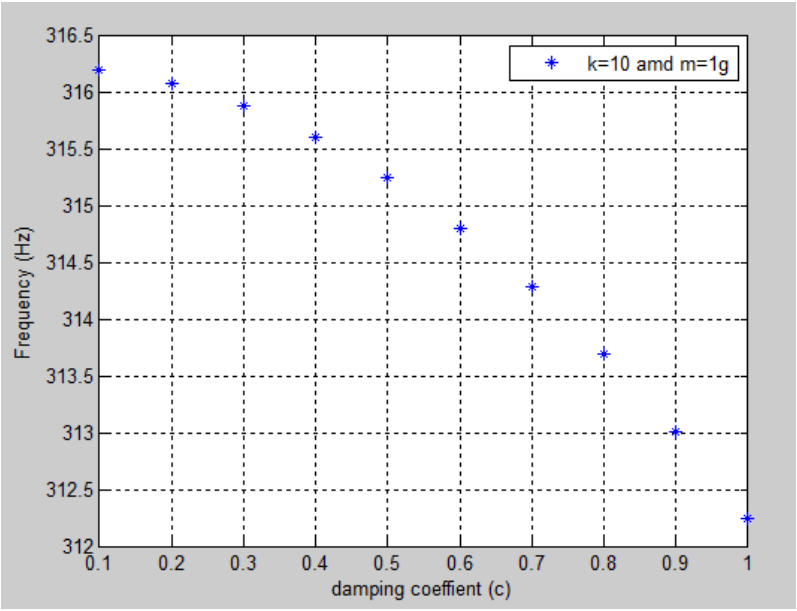

Figure 4.8: Damped vibration frequencies for various damping coefficient (c_d).

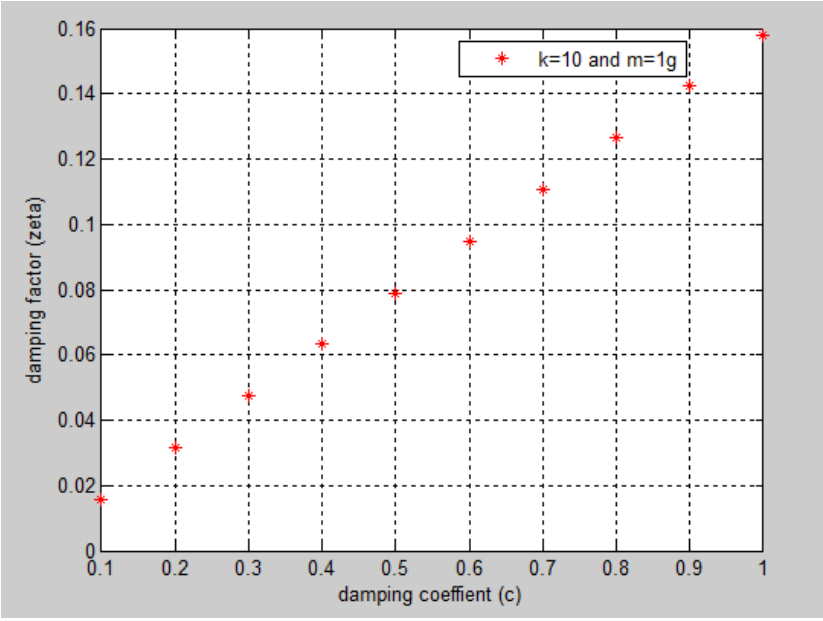

Figure 4.9: Change in ξ with change in damping coefficient (c_d).

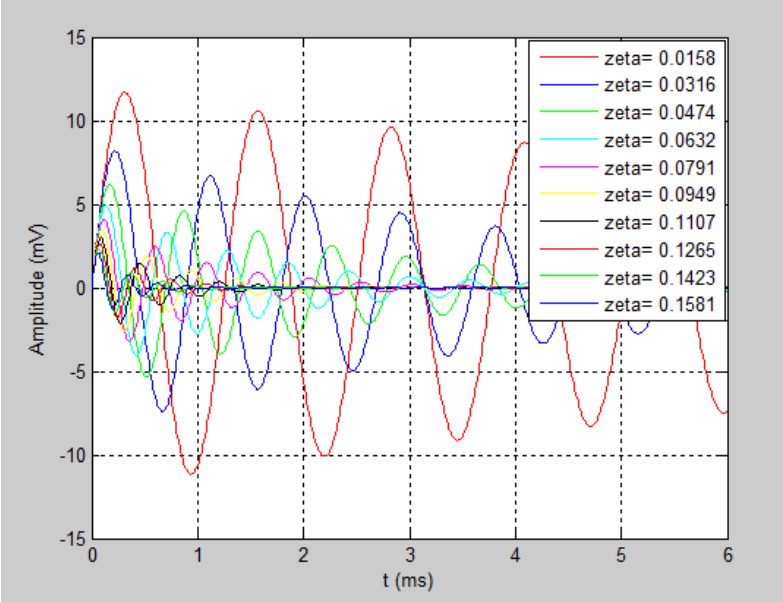

Figure 4.10: Amplitude of damped vibrations.

C. Changing mass (m):

Now to generate damped vibration frequencies, the mass (m) is changed, while the spring stiffness (k) and damping coefficient (ξ) is kept constant. To obtain the damped vibration frequencies, the mass was varied from 1g to 10g.Figure 4.11 shows the damped vibration frequencies generated w.r.t. change in mass (m). Figure 4.12 shows the change in damping factor (ξ) with change in mass (m). As seen from both the figures the damped vibration frequencies increase while damping factor (ξ) decreases as mass is increased. Figure 4.13 shows the amplitude of damped vibration frequencies generated. The resulting range of frequencies generated is from 300 Hz to 1000Hz.

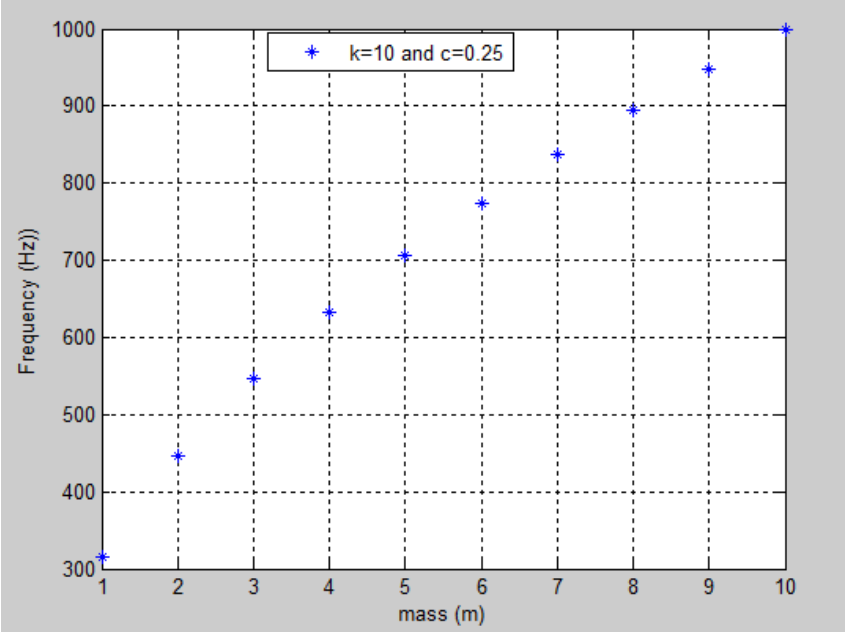

Figure 4.11: Damped vibration frequencies generated w.r.t. mass (m).

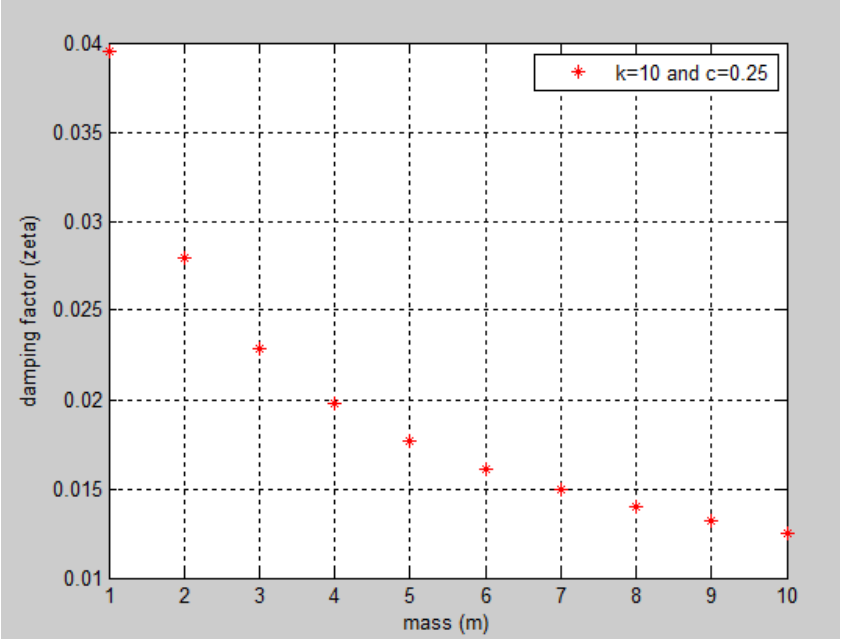

Figure 4.12: Change in ξ with change in mass (m).

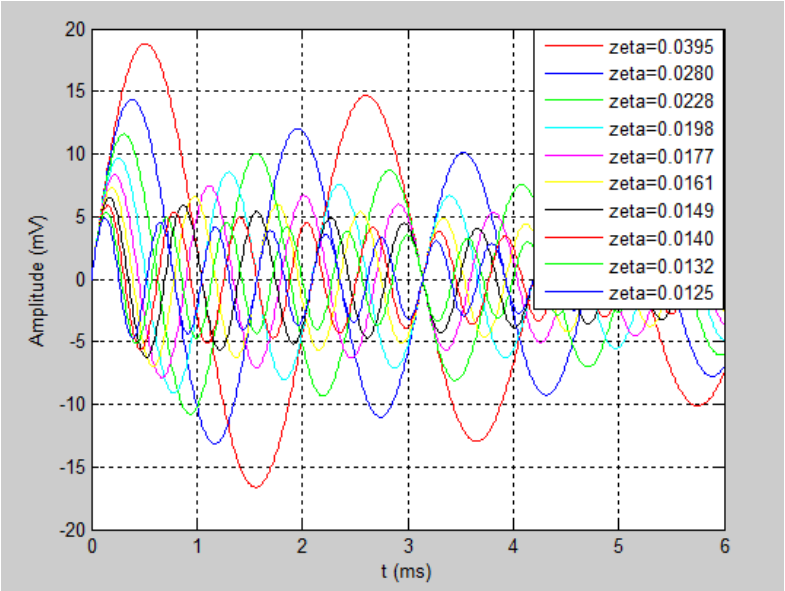

Figure 4.13: Amplitude of damped vibrations w.r.t. change in mass (m).

As seen from Figures 4.5 to 4.13, the significant change in frequencies are obtained for the change in spring stiffness (k) and mass (m). Thus the input frequency range that has been selected for detection is from 300Hz to 3100Hz. The modulated sensor output signal from photodiode (PD) is further demodulated using the RF band pass filter (RFBPF) and frequency demodulation system as shown in Figure 4.14.

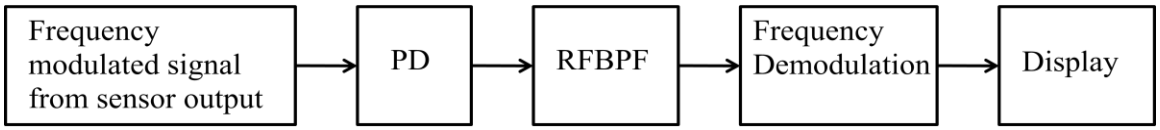

Figure 4.14: FM Demodulation system to detect vibration signals.

Thus the output of photodetector (PD) is FM signal but with different beat frequencies and frequency deviations. Different frequency modulated signals were passed through

demodulator system for further processing. The output from RFBPF is then mixed with local oscillator in a mixer as shown in Figure 4.15.

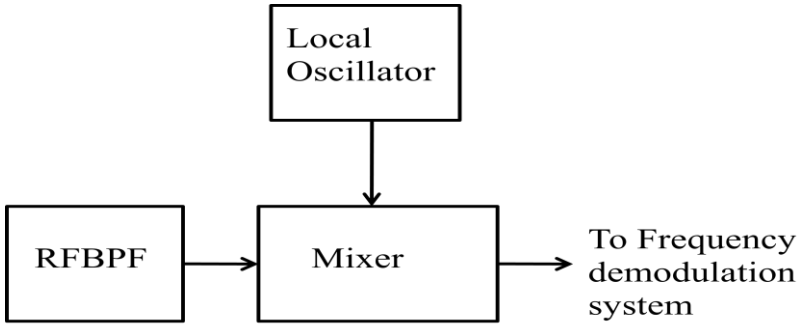

Figure 4.15: Downconversion of FM signal.

The FM signal from mixer is a downconverted approximation of beat frequency. This signal is then demodulated using frequency demodulation system (phase lock loop detector) to detect the damped vibration signal. The input and output signal of detected damped frequencies are shown in Figure 4.16.

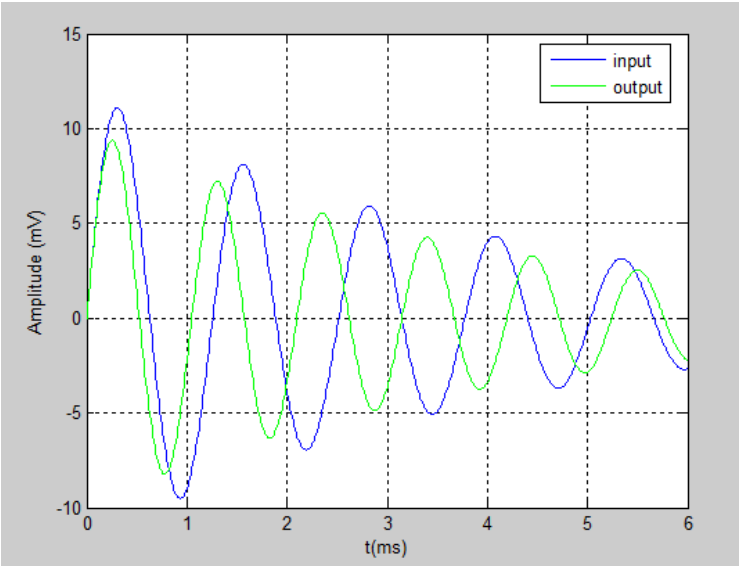

(a) f_d=500Hz

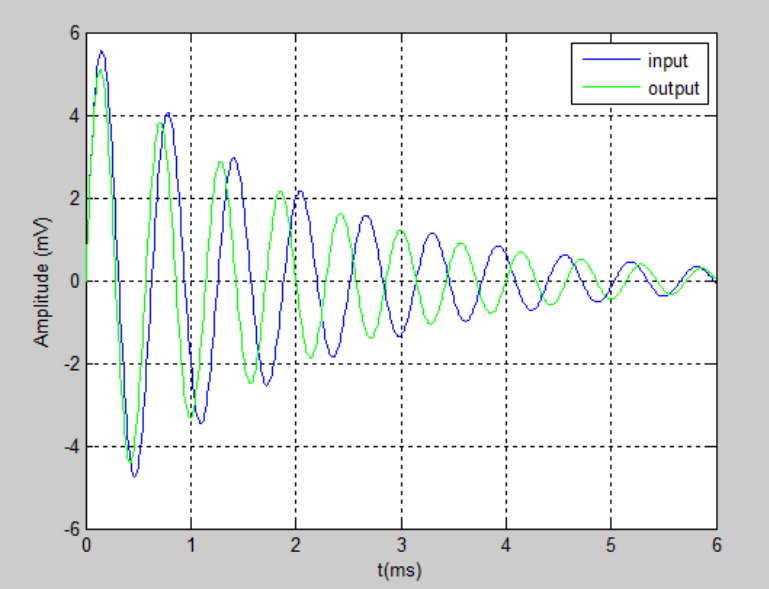

(b) f_d=1000 Hz

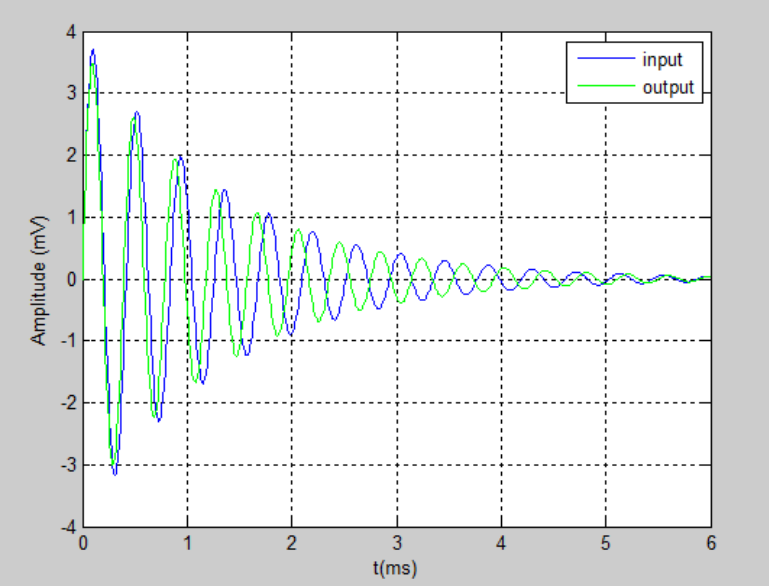

(c) f_d=2000Hz.

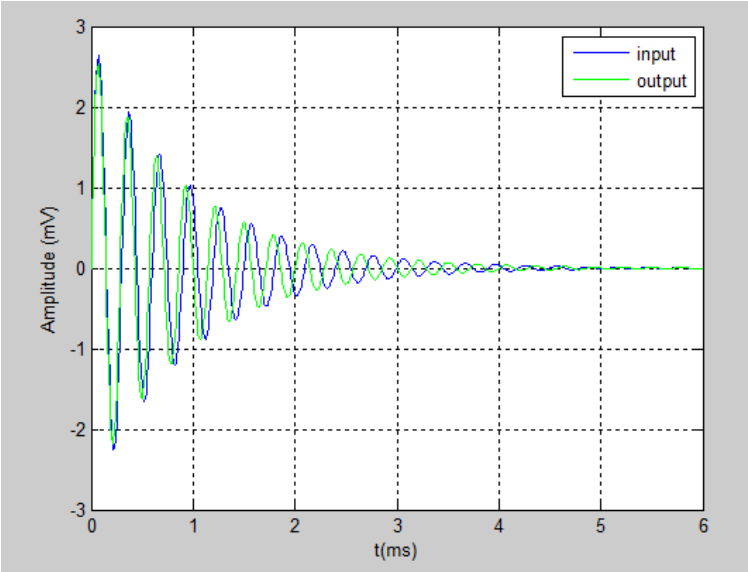

(d) f_d =3000Hz

Figure 4.16: Detected damped vibration signals.

Figures 4.16 (a), (b), (c), and (d) show the input and output signal for f_d=500Hz, f_d =1000 Hz, f_d =2000Hz, and f_d =3000 Hz, respectively. The percent error between amplitude of input and output signal is 18% while the phase shift is 16.093^o. The amplitude of output signal is attenuated due to phase lock loop detector used to demodulate the FM signal. The phase is observed due to polarization effect produced by applied vibration. Table 4.1 shows the amplitude of output signal for input damped vibration signals applied to the fiber.

Table 4.1: Amplitude of output signal for input damped vibrations.

Input Damped Frequency (Hz)	Amplitude of output signal (Loss in dB)
100	21.4

300	21.4
400	21
500	9.5
800	8.1
1000	7.4
1200	6.6
1500	5.8
2000	5.5
2300	4.9
2700	4.2
3000	3.9

As seen for Table 4.1 the signal attenuation was high for lower frequencies, while it was low for higher frequencies. This was observed because the demodulator used in simulation did not simulated lower frequency signals and thus showed high attenuation in the output signals. Figure 4.17 shows the plot for damped vibration frequencies v/s attenuation in the output signal.

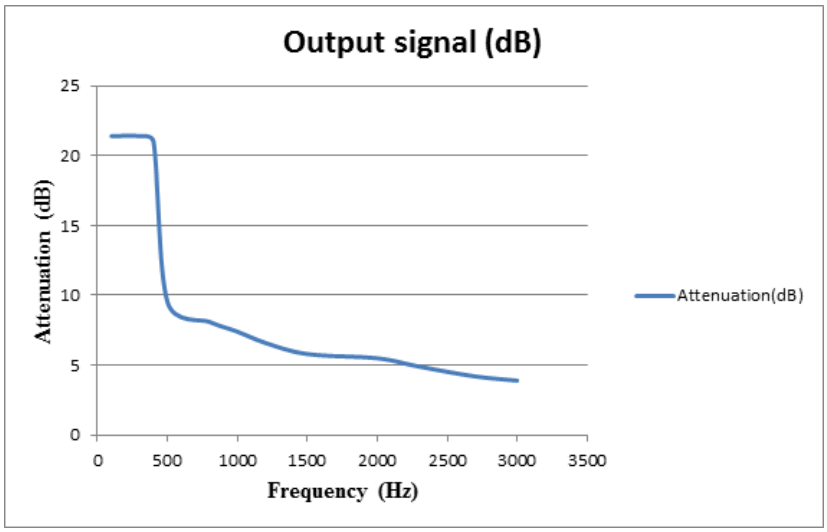

Figure 4.17: Damped vibration frequencies v/s attenuation (dB)

The range of frequencies that is detected from the simulation results is from 500Hz to 3000Hz. The experiment was conducted to verify the method proposed. The experimental results are discussed in chapter 5.

Chapter-5

Experimental Results

5.1 Experimental Setup

Figure 5.1 and 5.2 shows the schematic of the experimental setup and actual experimental setup used, respectively. The laser cavity is formed using the SMF, EDF, FBG and 3dB coupler. The FGB is spliced between 3-dB coupler and WDM. It has the reflectivity of 96.04%, center wavelength of 1549.08 nm, and bandwidth of 0.41nm. Portion of SMF and EDF are spliced to two ends of 3dB coupler. The lengths of SMF and EDF are 2m and 1m, respectively. When light with a wavelength of 980nm pump power is launched into the resonant cavity, multilongitudinal modes are produced within the reflected bandwidth of the FBG. Several beat frequency signals are generated by beating any two modes in the resonant cavity. In the presence of damped vibrations, the strain experienced by the fiber changes the length of the cavity which changes the beat frequency.

The damped vibrations are produced using the principle of cantilever beam. The schematic diagram for producing damped vibrations is shown in Figure 5.3. The fan connected to the frequency oscillator act as a load on the ruler (cantilever beam). This applied load is an external force that subjects ruler to deflect. When this force is removed the inertia keeps the ruler in motion. Thus the ruler vibrates to its characteristic frequency and produces damped vibrations. The range of damped vibration frequencies obtained is

from 100Hz to 2000Hz. The fiber which is wrapped around the ruler, experiences strain due to these damped vibrations.

A pulse from optical time-domain reflectometer (OTDR) is sent through WDM into the laser cavity. As explained in chapter 3, the multilongitudinal modes are generated in the cavity. The strain experienced by fiber due to applied damped vibration changes the beat frequency signals. The signal output from the sensor is detected by OTDR in the form attenuation in dB. The OTDR measures the attenuation of signal due to strain on fiber with applied damped vibrations.

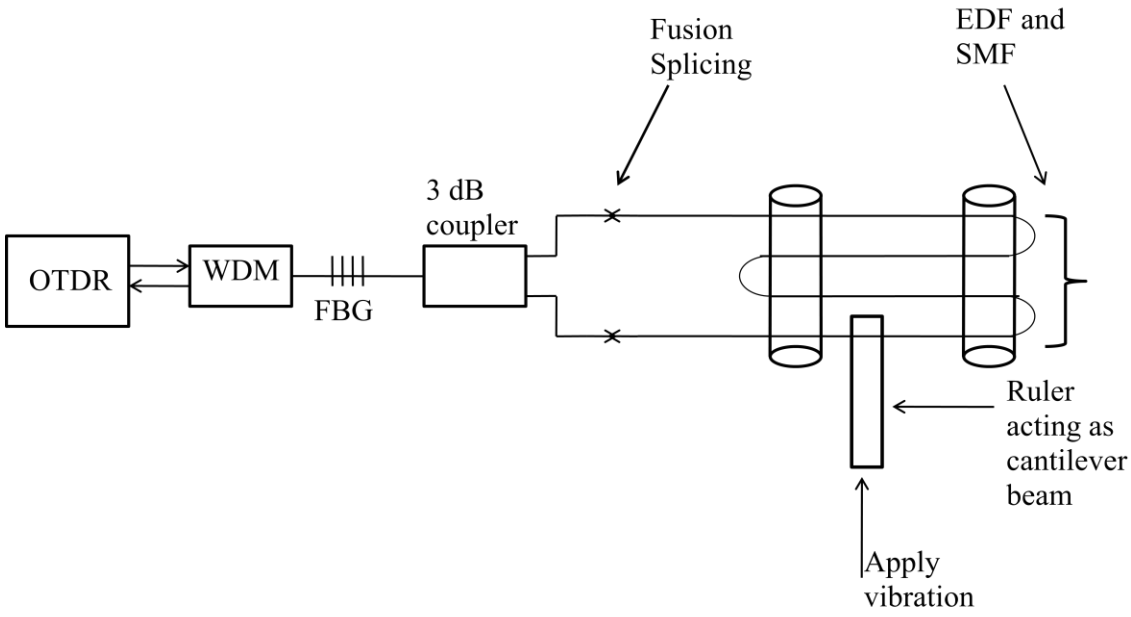

Figure 5.1: Schematic of experimental setup.

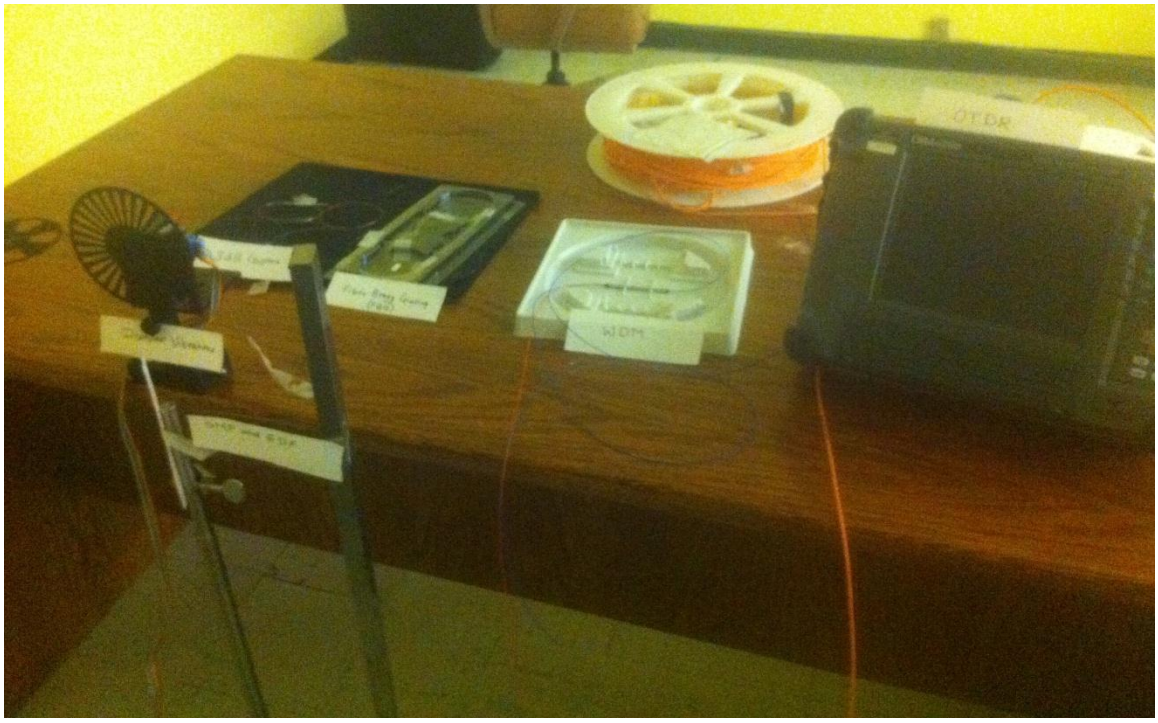

Figure 5.2: Experimental setup in Lab.

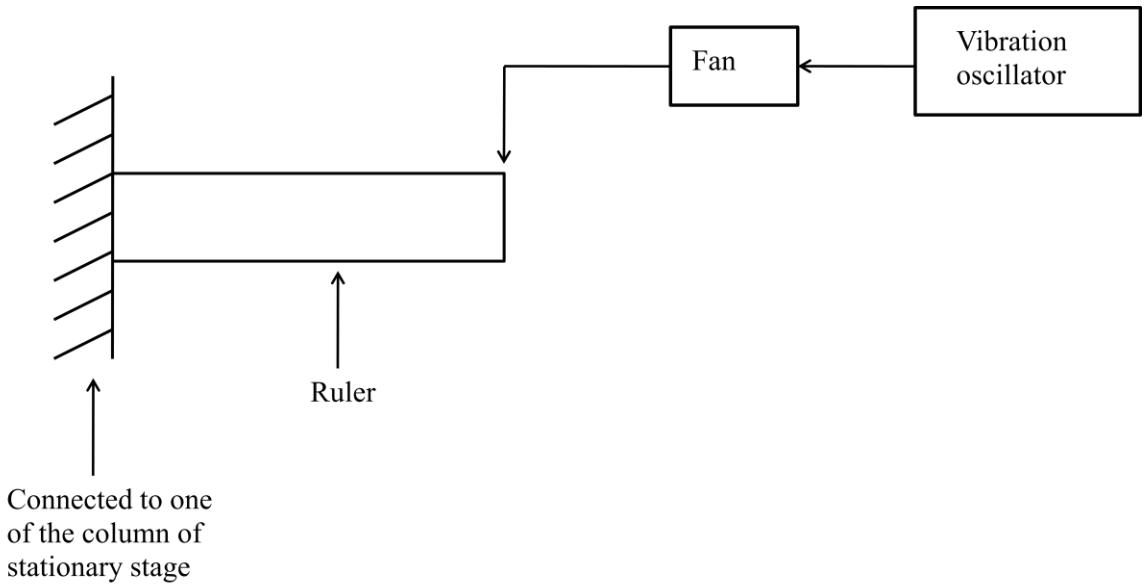

Figure 5.3: Schematic of generation of damped vibrations.

5.2 Experimental Results

In the experiment conducted,the sensor output was observed on OTDR for different time instances and displacement of ruler which was repeated three times. The reason for repetition was to check the validation of detected damped vibration frequencies. Table 5.1 shows the attenuation of the signal (dB) for various damped frequencies being applied on the sensor. The averages for all the three repetition are being calculated in the table.

Table 5.1: Attenuation of signals (dB) for various damped frequencies.

Time						
T1						
	Displacement (m)		Amplitude (Loss in dB)			
		Frequency (Hz)	Rp1	Rp2	Rp3	Average
	0.05	500	13.67	13.51	13.11	13.43
		1000	11.1	10.98	10.88	10.98
		1500	9.68	9.56	9.49	9.57
		2000	8.57	8.40	8.31	8.42
	0.06	500	11.26	11.09	10.97	11.11
		1000	7.04	6.99	6.91	6.98
		1500	5.85	5.71	5.5	5.68
		2000	3.73	3.6	3.55	3.62
T2						
	Displacement (m)		Amplitude (Loss in dB)			
		Frequency (Hz)	Rp1	Rp2	Rp3	Average
	0.05	500	11.25	11.08	10.98	11.1
		1000	10.76	10.68	10.66	10.7
		1500	7.98	7.8	7.75	7.84
		2000	6.45	6.24	6.19	6.29
	0.065	500	9.63	9.48	9.23	9.44

		1000	6.89	6.78	6.71		6.79
		1500	4.56	4.49	4.36		4.47
		2000	3.21	3.11	3.03		3.11
T3							
	Displacement (m)		Amplitude (Loss in dB)				
		Frequency (Hz)	Rp1	Rp2	Rp3		Average
	0.05	500	10.59	10.37	10.1		10.35
		1000	9.89	9.75	9.7		9.78
		1500	5.8	5.71	5.64		5.71
		2000	4.95	4.82	4.69		4.82
	0.07	500	8.87	8.77	8.69		8.77
		1000	4.98	4.91	4.89		4.92
		1500	3.84	3.7	3.51		3.68
		2000	2.9	2.78	2.64		2.77

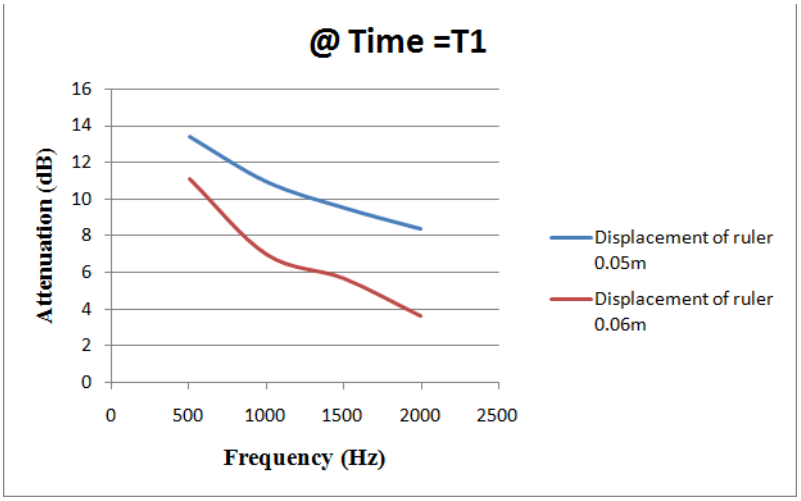

Figure 5.4: Average of loss in signal (dB) for different displacements and damped vibration frequencies at time T1.

As seen from Figure 5.4 the displacement of ruler from the stage column was taken as 0.05m and 0.06m for various damped frequencies. It is been observed that for

large displacement the strain experience by fiber is more and so the attenuation in signal is low. The signal attenuation was observed for frequencies at 500Hz, 1000Hz, 1500Hz and 2000Hz.

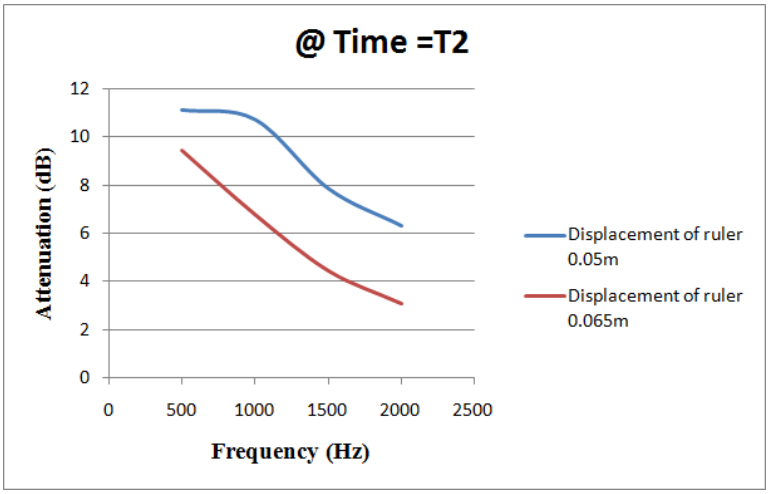

Figure 5.5: Average of loss in signal (dB) for different displacements and damped vibration frequencies at time T2.

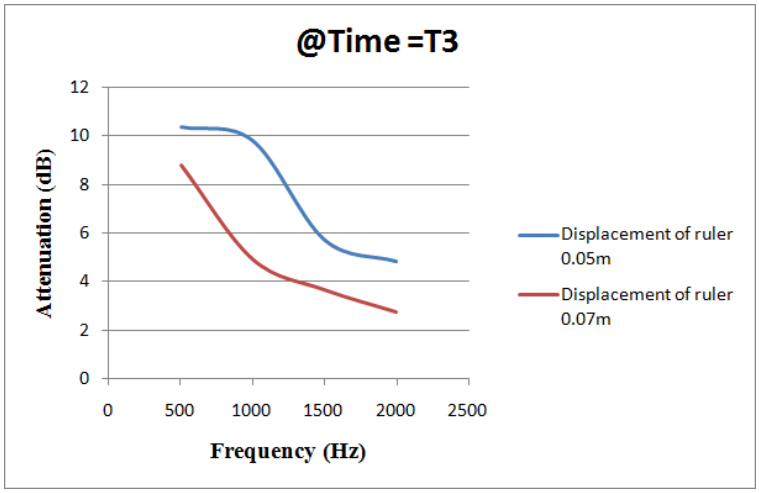

Figure 5.6: Average of loss in signal (dB) for different displacements and damped vibration frequencies at time T3.

Figures 5.5 and 5.6 shows the attenuation of signal at different time instances T2 and T3, respectively. The ruler displacement from stage column was taken as 0.05m, 0.06m, 0.065m and 0.07m. It has been observed that, as displacement of ruler from stage column and the frequencies were increased, the attenuation of signal decreased. This was observed because the length of cavity and beat frequencies changed which changed number of modes produced in the cavity. Thus with increase in amplitudes and frequencies the number of modes decreased and so the attenuation in the signal.

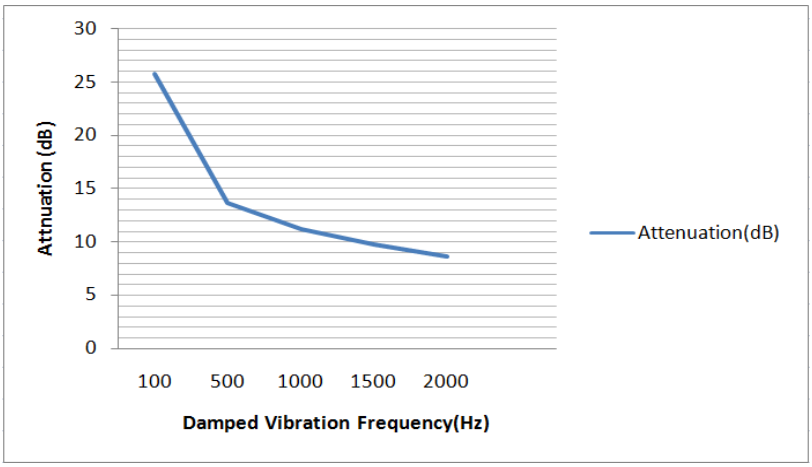

Figure 5.7: Damped vibration frequency (Hz) v/s attenuation (dB).

As seen from Figure 5.7 at 100Hz high signal attenuation of 25.783 dB is observed, while for all other frequencies the attenuation of the signal was lower than 15dB. At lower frequencies the numbers of modes produced in the cavity were higher and so the loss in signal was higher.

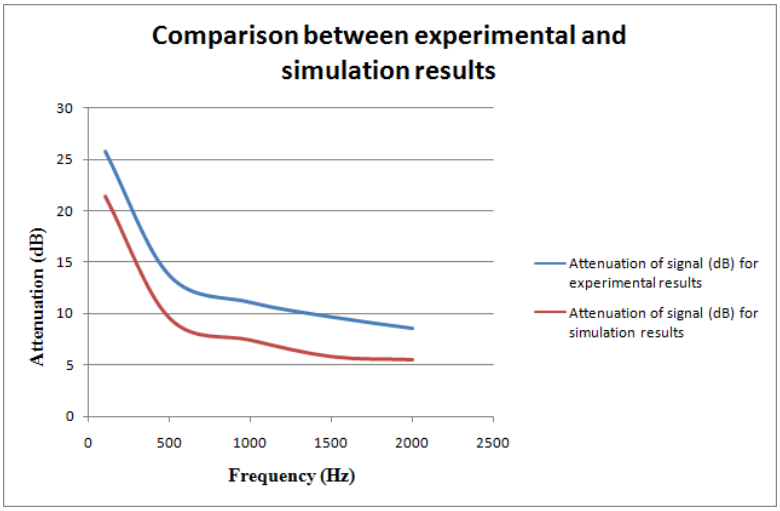

Figure 5.8: Comparison between experimental and simulation results.

Figure 5.8 shows the comparison between experimental and simulation results. Both experimental and simulation results show the high attenuation for lower frequencies and lower attenuation for higher frequencies. For frequencies below 500Hz the difference in attenuation is about 5dB while for frequencies above 500Hz the attenuation difference is about 4dB. The simulation results show the lower signal attenuation compared to experimental results. This is due to the losses in fibers and connectors not being considered in simulation results. However in experimental results these losses are inherent. From the experimental results damped vibration frequencies have been observed from 500Hz to 2000Hz. At the same time, the analytical simulation method resulted in the damped vibration frequencies 500Hz to 3000Hz. This difference in the frequency range is due to different methods used for generating damped vibration frequencies and demodulation techniques. For analytical simulations of damped vibration frequencies, the beat frequency and frequency modulation/demodulation method has been

used. For experiment results an OTDR was used to observe the attenuation of the signal due to applied vibrations.

Chapter 6-Conclusion

A new method for detection of damped vibrations has been successfully experimented. The system used is simple and cost effective as the sensor is made of SMF, FBG, EDF fibers and 3dB coupler. The damped vibrations from 500Hz to 2000Hz have been detected and measured successfully. The experimental results showed that the attenuation of signal was lower for higher frequencies. The simulation results showed that the range of damped vibration frequencies detected were from 500Hz to 3000Hz. It also showed the percent error of 18% between amplitude of input and output signals. The phase shift of 16.093^{o} was also observed. The percent error and phase shift were observed as the polarization effects on fiber were not considered. Both experimental and simulation results show the high attenuation for lower frequencies and lower attenuation for higher frequencies. For frequencies below 500Hz the difference in attenuation is about 5dB while for frequencies above 500Hz the attenuation difference is about 4dB. However in experimental results these losses are inherent.This validates the proposed method in this thesis.

In the experiment conducted, OTDR was used to measure signal attenuation to detect damped vibrations. But for further analysis and improve accuracy, signal processing is necessary. This can be done using photodiode, filters, and demodulator system. The polarization maintaining fiber can be used to compensate the polarization effect in the experiment. Since the experiment was conducted in the laboratory environment the strain on the fiber due to change in temperature of stage column was not considered. For more accurate results, the analysis for temperature compensation has to

be taken into consideration. Damped vibration sensors can be used for applications like monitoring earthquake, structural damages in civil infrastructure like highways, bridges, hydroelectric dam and heavy electromechanical equipments.

References

[1] Shizhuo Yin, Paul B. Ruffin and Francis T.S. Yu, ed., *Fiber Optic Sensor*, CRC Press, New York, 2008.

[2] E.UDD, ed., *Fiber Optic Sensors: An Introduction for Engineers and Scientists*, Wiley, New York, 1991.

[3] E. Udd, ed., *Fly-by-light*, Proc. SPIE, 2295, 1994.

[4] Babs. R. Soller, "Design of Intravascular Fiber optic blood gas senor", IEEE Engineering in Medicine and Biology, pp.327-335, July. 1994.

[5] Shizhuo Yin, Paul B. Ruffin and Francis T.S. Yu, ed., *Fiber Optic Sensor*, CRC Press, New York, 2008.

[6] P. L. Fuhr and D. R. Nuston, "*Multiplexed fiber optic pressure and vibration sensors for hydroelectric dam monitoring*," Smart Mater. Struct., vol. 2, pp. 130–263, Dec.1993.

[7] H. L. Rivera, J. A. García-Souto, and J. Sanz, "*Measurements of mechanical vibrations at magnetic cores of power transformers with fiberopticinterferometric intrinsic sensor*," IEEE J. Sel. Topics Quantum Electron., vol. 6, no. 5, pp. 788–797, Sep./Oct. 2000.

[8] Y. Shindo, T. Yoshikawa, and H. Mikada, "*A large scale seismic sensing array on the seafloor with fiber optic accelerometers*," in Sensors, Proc. IEEE, 2002, vol. 2, pp. 1767–1770, Nov. 2002.

[9] T. K. Gangopadhyay and P. J. Henderson, "*Vibration: History and measurement with an extrinsic Fabry-Perot sensor with solid-state laser interferometry*," Appl. Opt., vol. 38, no. 12, pp. 2471–2477, Apr. 1999.

[10] K. P. Koo and A. D. Kersey, "*Bragg grating-based laser sensors systems with interferometric interrogation and wavelength division multiplexing*," J. Lightw. Technol., vol. 13, no. 7, pp. 1243–1249, Jul. 1995.

[11] M. A. Davis, A. D. Kersey, J. Sirkis, and E. J. Friebele, "*Shape and vibration mode sensing using fiber optic Bragg grating array*," Smart Mater. Struct., vol. 5, pp. 759–765, Dec. 1996.

[12] M. Kimura and K. Toshima, "*Vibration sensor using optical-fiber cantilever with bulb-lens*," Sens. Actuators A, Phys., vol. 66, pp. 178–193, Feb. 1998.

[13] S. Liu, Z. Yin, R. Gu, L. Zhang, L. Gao, X. Chen, and J. Cheng, "*Multi-longitudinal mode fiber-ring laser for strain measurement*," Optical Engineering, pp. 054401-1–054401-5, May. 2011.

[14] M. Lequime, "*Fiber sensors for industrial applications*," in Proceedings of the 12th International Conference on Optical Fibre Sensors, vol. 16 of OSA Technical Digest Series, pp. 66– 71, OSA,Washington, DC, USA, Oct. 1997.

[15] R.Medlock, "*Fibre optics in process-control*," Control Instrum, vol. 21, no. 4, pp. 105–108, 1989.

[16] V. Demjanenko, R. A. Valtin, M. Soumekh et al., "*A noninvasive diagnostic instrument for power circuit breakers*," IEEE Transactions on Power Delivery, vol. 7, no. 2, pp. 656–663, Apr. 1992.

[17] Fidanboylu, K.andEfendioglu, H. S, "*Fiber Optic Sensors and their Applications*" 5th International Advanced Technologies Symposium (IATS'09), May. 2009.

[18] Yoany Rodríguez García, Jesús M. Corres and Javier Goicoechea. "*Vibration Detection Using Optical Fiber Sensors*", Journal of Sensors, Jul. 2010.

[19] U. Gunasilan, "*Operative factors contributing to the selection of fiber-optic techniques for remote measurement of strain/stress*," in Proceedings of the IEEE 9th International Conference on Computer and Information Technology, Middlesex University Dubai, Oct. 2009.

[20] J. Hecht, Understanding Fiber Optics, Pearson Prentice Hall, NJ, USA, 2006.

[21] W. Horsthuis and J. Fluitman, "*Sensitivity dependence on number of bends in a microbend pressure sensor*," NTGFachberichte, vol. 79, pp. 147–152, 1982.

[22] Shizhuo Yin, Paul B. Ruffin and Francis T.S. Yu, ed., *Fiber Optic Sensor*, CRC Press, New York, 2008.

[23] G. Murtaza, S. L. Jones, J. M. Senior, and N. Haigh, "*Loss behavior of single-mode optical fiber microbend sensors*," Fiber and Integrated Optics, vol. 20, no. 1, pp. 53–58, Oct. 2001.

[24] J.W. Berthold III, "*Historical review of microbend fiber-optic sensors*," Journal of Lightwave Technology, vol. 13, no. 7, pp.1193–1199, Jul. 1995.

[25] M. Kuhn, "*Curvature loss in singlemodefibres with lossy jacket*," Archiv fur Elektronik und Ubertragungstechnik, vol. 29, no. 9, pp. 400–402, 1975.

[26] N. K. Pandey and B. C. Yadav, "*Embedded fibre optic microbend sensor for measurement of high pressure and crack detection*," Sensors and Actuators A, vol. 128, no. 1, pp. 33–36, Jan. 2006.

[27] G. Perrone and A. Vallan, "*A low-cost optical sensor for noncontact vibration measurements*," IEEE Transactions on Instrumentation and Measurement, vol. 58, no. 5, pp. 1650–1656, May 2009.

[28] Yoany Rodríguez García, Jesús M. Corres and Javier Goicoechea. "*Vibration Detection Using Optical Fiber Sensors*", Journal of Sensors, Jul. 2010.

[29] V. S. Sudarshanam and R. 0. Claus, "*Split-cavity cross-coupled extrinsic fiber-optic interferometric sensor*", Optics Letters, Vol. 18, No. 7, pp.543-545, Apr. 1993.

[30]T. K. Gangopadhyay, S. Chakravorti, S. Chatterjee, and K. Bhattacharya, "*Multiple fringe and nonsinusoidal signals obtained froma fiber-optic vibration sensor using an extrinsic Fabry-Perot interferometer*," Measurement Science and Technology, vol. 16, pp. 1075–1082, May. 2006.

[31] S. Pullteap, H. C. Seat, and T. Bosch, "*Modified fringecounting technique applied to a dual-cavity fiber Fabry-Perot vibrometer*," Optical Engineering, vol. 46, no. 11, Article ID 115603, Dec. 2007.

[32] T. Yoshino, K. Kurosawa, K. Itoh, and T. Ose, "*FiberopticFabry-Perot Interferometer and its sensors applications*", Journal of Quantum Electronics, vol. 18, no. 4, pp. 626–665, Oct. 1982.

[33] J. M. Corres, J. Bravo, F. J. Arregui, and I. R. Matias, "*Unbalance detection in electrical engines using an in-line fiber etalon*", in Proceedings of the 4th IEEE Conference on Sensors, pp. 1347–1350, Irvine, CA, USA, Nov. 2005.

[34] http://en.wikipedia.org/wiki/Fiber_Bragg_grating

[35] Yoany Rodríguez García, Jesús M. Corres and Javier Goicoechea. "*Vibration Detection Using Optical Fiber Sensors*", Journal of Sensors, Jul. 2010.

[36] G.Meltz,W.W.Morey,W. H. Glenn, and J.D. Farina, "*In-fiber Bragg-grating temperature and strain sensors*," in Proceedings of the 34th International Instrumentation Symposium, pp. 239– 242, May 1988.

[37] G. Meltz, W. W. Morey, W. H. Glenn, and J. D. Farina, "I*nfiberbragg-grating sensors,"* in Proceedings of the Optical Fiber Sensors, vol. 2, pp. 163–166, 1988.\

[38]M. A. Davis and A. D. Kersey, "*All-fibre Bragg grating strainsensor demodulation technique using a wavelength division coupler*," Electronics Letters, vol. 30, no. 1, pp. 75–77, Jan. 1994.

[39] A. Cusano, A. Cutolo, J. Nasser, M. Giordano, and A. Calabr "*Dynamic strain measurements by fibre Bragg grating sensor*", Sensors and Actuators A, vol. 110, no. 1–3, pp. 276–281, Oct. 2004.

[40] A. Laudati, F. Mennella, M. Giordano, G. D'Altrui, C. CalistiTassini, and A. Cusano, "*A Fiber-Optic Bragg Grating Seismic Sensor*", IEEE Photonics Technology Letters, Vol. 19, No. 24, pp. 1991- 1993, Dec. 2007.

[41] J. Leng and A. Asundi, "*Structural health monitoring of smart composite materials by using EFPI and FBG sensors*," Sensors and Actuators A, vol. 103, no. 3, pp. 330–340, Jan. 2003.

[42] K.-T. Lau, L. Yuan, L.-M. Zhou, J.Wu, and C.-H.Woo, "*Strain monitoring in FRP laminates and concrete beams using FBG sensors*," Composite Structures, vol. 51, no. 1, pp. 9–20, Nov. 2001.

[43] Y. B. Lin, C. L. Pan, Y. H. Kuo, K. C. Chang, and J. C. Chern, "*Online monitoring of highway bridge construction using fiber Bragg grating sensors*," Smart Materials and Structures, vol. 14, no. 5, pp. 1075–1082, Sept. 2005.

[44] P. Moyo, J. M. W. Brownjohn, R. Suresh, and S. C. Tjin, "*Development of fiber Bragg grating sensors for monitoring civil infrastructure*," Engineering Structures, vol. 27, no. 12, pp. 1828–1834, Oct. 2005.

[45] Clarence W.de Silva, *Vibration: Fundamental and Practice*, CRC Press, New York, 2000.

[46] http://en.wikipedia.org/wiki/Damping

[47] Ziyi Zhang and XiaoyiBao, "*Continuous and Damped Vibration Detection Based on Fiber Diversity Detection Sensor by Rayleigh Backscattering*", J. Lightwave technology, Vol. 26, No. 7, pp-832-838, Apr.2008.

[48] S. Liu, Z. Yin, L. Zhang, L. Gao, X. Chen, and J. Cheng, "*Multi-longitudinalmode fiber laser for strain measurement*," Opt. Lett., vol. 35,no. 6, pp. 835–837, Mar. 2010.

[49]S. Liu, Z. Yin, R. Gu, L. Zhang, L. Gao, X. Chen, and J. Cheng, "*Multi-longitudinal mode fiber-ring laser for strain measurement*," Optical Engineering, pp. 054401-1–054401-5, May. 2011.

[50] S. Liu, L. Gao, Z. Yin, L. Zhang,X. Chen, "*Multi-Longitudinal Mode Fiber Laser Sensor Combining the Fiber Bragg Grating Reflector*,"Communications and Photonics Conference and Exhibition (ACP), 2010 Asia, pp.96-96 Dec.2010.

[51]Z. Yin, L.Gao, S.Liu, L.Zhang, F.Wu, L.Chen, and X.Chen, "*Fiber Ring Laser Sensor for Temperature Measurement*," J. Lightwave Technology, Vol.28, No. 23, Dec. 2010.

[52] L.Gao, S.Liu,Z.Yin, H.Zhang, L.Chen, L.Zhang, X.Chen,"*Fiber Laser Sensor With Beat Frequency Demodulation*", Optical Communications and Networks (ICOCN 2010), pp-29-30, Oct.2010.

[53] L. Gao, S. Liu, Z. Yin, L. Zhang, X. Chen, and J. Cheng, "*Fiber –optic Vibration Sensor Based on Beat Frequency and Frequency-Modulation Demodulation Technique* ," IEEE Photonics Technology Lett., vol. 23,no. 1, pp. 18–20, Jan. 2011.

[54] http://en.wikipedia.org/wiki/Vibration